PERGAMON

Progress in Energy and Combustion Science 27 (2001) 547–585

PROGRESS IN ENERGY AND COMBUSTION SCIENCE

www.elsevier.com/locate/pecs

Gaseous diffusion flames: simple structures and their interaction

A. Cavaliere[a,*], R. Ragucci[b]

[a]*Dip. di Ingegneria Chimica, Università degli Studi Federico II, Piazzale Tecchio 80, 80125 Naples, Italy*
[b]*Istituto di Ricerche sulla Combustione C.N.R., Naples, Italy*

Received 10 November 1999; accepted 21 November 2000

Abstract

This is a synoptic overview of a selection of works dealing with single diffusive structures, with their mutual interaction in simple flows and their statistical modeling in complex flows. The focus is on reacting conditions pertaining to gaseous diffusion flames, but isothermal structures are also described when they are of some conceptual interest. This paper considers only few representative works for each subject, which are functional in explaining the key characteristics of the diffusive structures. The extension, given to single subjects, is not weighed according to the number of related publications but on the relevance to the basic understanding of the general framework concerning diffusion flames. One-dimensional structures are first discussed. They are ordered according to the number of balance equation terms needed for their description. Two-dimensional (2D) structures are then introduced following an order based on their convolution level. Some pioneering work on three-dimensional structures is further quoted. The temporal evolution of simple structures in quiescent or simple flowing 2D systems is considered. The latter case is exploited to present classification of diffusion-controlled mixing regimes. Modeling characterization approach of turbulent diffusion flames is also described in order to yield a self-sufficient didactic presentation. The approach based on the flame surface density model is specifically discussed because of its potential use in the determination of qualitative and quantitative features of simple diffusion flames.

Keywords: Diffusion flames; Mixing; Structure

Contents

* Corresponding author. Tel.: +39-81-768-2264; fax: +39-81-513-6936.
E-mail address: antcaval@unina.it (A. Cavaliere).

0360-1285/01/$ - see front matter
PII: S0360-1285(00)00031-9

1. Introduction

Gaseous diffusion flames have been the main topic of numerous papers and many reviews. A rich capital of knowledge has been accumulated in a relatively disordered way because of the great momentum related to the subject from technological point of view with consequent haste to achieve significant results. Historically, Burke and Schumann [1] initiated the description of diffusion flames, with a remarkable study of two-dimensional (2D) laminar flames, and continued only years later with research related to one-dimensional (1D) diffusion flames [2,3]. In contrast studies on premixed laminar flames have followed an opposite route facing, during the last two centuries, the gradual increase of physical, chemical and mathematical difficulties [4].

The early analyses of 1D configurations relative to the experimental [2], theoretical [5–7] and numerical studies [8] have branched new research ways and have been added to the previous 'corpus' of knowledge. Fruitful intersection with other autonomous fields like fluid-dynamics (e.g. stirring, mixing) [9–11] or mathematics (e.g. percolation [11], chaos [12]) or chemical kinetics (e.g. new oxidative schemes for low temperature and rich conditions), have generated different types of analyses of gaseous diffusion flames. All of them refer obviously to the same physics and chemistry, but sometimes they are difficult to be recognized by neophytes, who deal for the first time with this topic. In other words, the large body of literature obscures, at the first approach, the understanding of the mechanistic aspects of the process.

Review papers are also necessarily confined by the authors to one methodological approach or to narrow classes of flame configurations, which are themselves rich of different aspects (or which deal with numerous types of fuels and external conditions). It is hence difficult to review exhaustively all the papers, published in a single field, and at the same time to consider different approaches or different configurations.

One purpose of the present paper is to offer a review, which tries to overcome this limit. In fact it covers a broad range of aspects and is intended as a sort of hypertext linking different specific reviews to which the reader is addressed for a deeper understanding of each subject. It is built as a systematic presentation of 'simple' diffusion flames ordered according to their complexity, expressed in terms of spatial dimensionality (one, two or three-dimensional (3D)), of numbers of balance terms added to diffusion (accumulation, convection, source terms) and of number of simple structural units examined (single, double, multiple mixing layers, etc.). Section 4 is completely devoted to this presentation.

Section 5 deals with interactions between simple diffusion structures in regimes which are more complex, but which have not the full characteristics of turbulent ones. These are the quiescent 2D fields and the 2D transitional regimes, for which numerical simulation and quantitative imaging are available.

Nomenclature

A	Strain rate
B	Stratification parameter or Dold number
C	Curvature
C_{sat}	Saturation factor
$\mathscr{D}$	Mass diffusivity
h_s	Sensitive enthalpy
h_i^0	Formation enthalpy of ith species
I	Integrated stretch rate
K	Stretch rate
K_{tot}	Total stretch rate
Le	Lewis number
l_f	Premixed flame thickness
M_i	Molecular weight of ith species
p	Pressure
Pr	Prandtl number
Sc	Schmidt number
SR	Stretch ratio
t	Time
T_p	Equilibrium maximum temperature
$\mathbf{n}$	Unity perpendicular vector
$\mathbf{v}$	Fluid-dynamic velocity
$\mathbf{v}^{tot}$	Total velocity
Y	Mass fraction of generic species
$\mathbf{w}$	Propagation speed
Z	Mixture fraction
Z_m	Overall mixture fraction
Z_{st}	Stoichiometric mixture fraction

Greek symbols

α	Thermal diffusivity
β	A conserved variable per unit mass
δ	Diffusive layer thickness
δ_m	Diffusive isothermal layer thickness
δ_m^{ns}	Unstretched diffusive layer thickness
δA	Surface element
δ_Z	Diffusive layer thickness at Z_{st}
δ_r	Physical reactive layer thickness
Δ_n	Interface separation distance
γ	Stretching factor
ν	Kinematic diffusivity
χ	Dissipation rate
ϕ	Diffusive flux
ρ	Density
ρ_i	Mass production rate for unit volume of ith species
σ	Reactive layer thickness in Z space
$\Sigma_{Z'}$	Surface density
ξ	Boltzmann variable

A classification of the possible interactions in these conditions is also given in the same section. This provides a classification guideline of fully turbulent regimes.

A schematic representation of the sub-topics is reported in a set of synthetic figures in order to make identification and memorization of the subject easier. This is the outstanding case of the 2D round jet flames, which is of great technological relevance and it has been presented in many classical combustion books [13–16]. Nevertheless, these flames are presented here only as an example of diffusion flame structure and are inserted in a single section together with wake flames.

Definitions of the less conventional quantities (like interface and intermaterial surface) are given in the following section together with more common definitions (conserved variable, mixture fraction). The most general approach to the analysis of diffusion flames is presented in Section 3 for the sake of completeness even though it is widely dealt in the literature.

Diffusion flames are commonly defined as processes in which oxidizer and fuel are completely separated and diffuse toward an oxidation region. It should be emphasized that this name (diffusion flame) is also used here for processes in which a minor part of the fuel undergoes mixing without significant reaction activity. More specifically, partially premixed flames are sometimes included in some regimes or structure descriptions, but it should be clear from the context that diffusion processes are dominant in determining their evolution.

2. Definitions

2.1. Conserved and material variables, tracers

A variable is conserved if it obeys a source-free balance equation; i.e. it is relative to a quantity which cannot be created or destroyed, but only convected and diffused. This statement is expressed in differential form according to the following equation, reported with classical notation as it can be found in many basic text books [13,14]

$$\rho\frac{\partial\beta}{\partial t} + \rho\mathbf{v}\cdot\nabla\beta - \nabla\cdot(\rho\,\mathscr{D}_\beta\nabla\beta) = 0 \tag{1}$$

in which β represents a conserved variable per unit mass.

According to basic physical principles, the total energy and the total mass are conserved. In contrast, the energy associated with a single species or the mass fraction of species are not generally conserved, because they can be converted in other forms of energy and in others kinds of molecular species, respectively. Other examples of conserved variables are the mass of an atomic species, if atomic reaction can be neglected, or the quantities, which are not conserved in principle, but which do not undergo significant conversions in specific cases (for instance inert species in complex reactive systems).

Conserved variables peculiar to the combustion field are obtained as a linear combination of some non-conserved

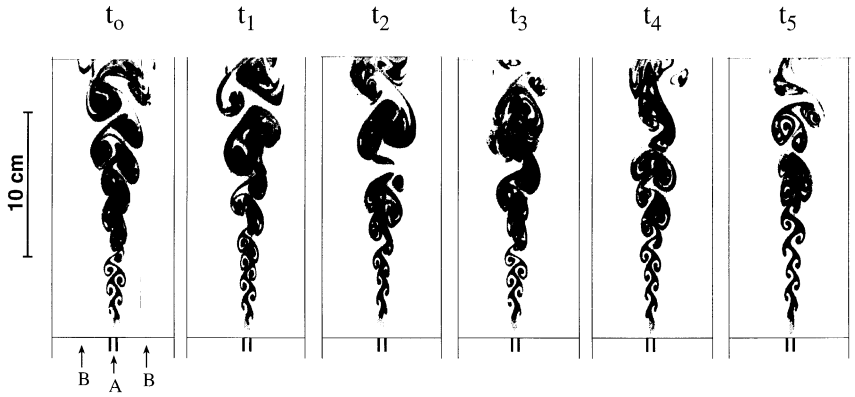

Fig. 1. Interfaces sequence of a transitional isothermal jet (after Cavaliere et al. [21]).

variables. They are described as 'coupling functions' or Schvab–Zel'dovich variables [13,14] and are generally used as a combination of mass fractions of the whole fuel and oxidizer, which can be thought as reacting in a single step and in a fixed stoichiometric ratio. Generalization of this kind of coupled–conserved variable also can be obtained for multi-component media and for combination of molecular species and formation enthalpy. In the latter case a free-source conservation equation of the total enthalpy (including of sensible and formation enthalpies) is considered.

A normalized form of a conserved variable can be defined, in terms of a mixture fraction, as

$$Z = \frac{\beta_l - \beta_{ox}}{\beta_f - \beta_{ox}} \tag{2}$$

subscripts l, f, ox, stand for local, fuel and oxidizer, respectively. Therefore, corresponding conserved variables (β_l, β_f, β_{ox}) are defined at all points of mixing flows (subscript l), in the unmixed fuel flow (subscript f) and in the unmixed oxidizer flow (subscript ox), respectively. It is of interest to note, according to the demonstration reported by Peters [4] (Appendix A), that:

1. this definition is also used in the case of partially premixed flames when some oxidizer is present in the fuel as a minor component and fuel is present in the oxidizer flow;
2. the definition is also used when the two streams are diluted with inert species;
3. the values of the mixture fractions, referred to different conserved variables, are equal when they diffuse with the same rate.

Mixture fraction (Z) complies with the same conservation equation of any conserved variable (β), since they differ for fixed quantities, ($\beta_{ox}/(\beta_f - \beta_{ox})$), disappearing in the differentiation and for a factor, $1/(\beta_f - \beta_{ox})$, which can be neglected because it is present in all the terms of the conservation equation. In other words, Eq. (1) applies also to the mixture fraction when the symbol β is changed with symbol Z.

The sum of the first two terms in Eq. (1), divided by the density, is designated in the literature as material or substantial derivative. It is cited in the following as $D(\cdot)/Dt$ and it defines a 'material' variable, β_M when Eq. (1) can be written as

$$\frac{D\beta_M}{Dt} = \frac{\partial \beta_M}{\partial t} + \mathbf{v}\cdot\nabla\beta_M = 0 \tag{3}$$

An example of material variable, which will be used in the following, is the mass fraction of a tracer. This last quantity is defined as an inert substance, uniformly dispersed in part of the flow, in such a weak concentration that the thermal and fluid-dynamic evolution of the flow is not altered.

In agreement with Ottino [17] the tracer should not only be non-diffusing but should also be transported at mean field velocity. In this way the tracer's mass fraction, Y_t, will be constant in time, and therefore the material derivative of Y_t will be zero.

It is quite difficult to produce this kind of tracer under experimental conditions in order to seed a gaseous flow also because the tracer cannot be a gas, as gases, by definition, diffuse. Neither can the tracer be a solid particle of such large dimensions to be unable to immediately respond to accelerations in the average flow. In effect the only tracer, which has features which are close to those described in the definition above, is a particle for which the Stokes number is less than unity [18] and for which the Schmidt number is greater than 1000 [19]. A particle, for instance, between 0.1 and 1 μm is sufficiently large in dimension to ensure that Brownian diffusion is low, but it is sufficiently small to immediately follow a flow. At times the term 'tracer' refers to a diffusive substance (generally featuring a molecular diffusion coefficient equal to the mean coefficient of the substances into which it must diffuse). In such cases it is always better to specify 'diffusive tracer' in order to avoid

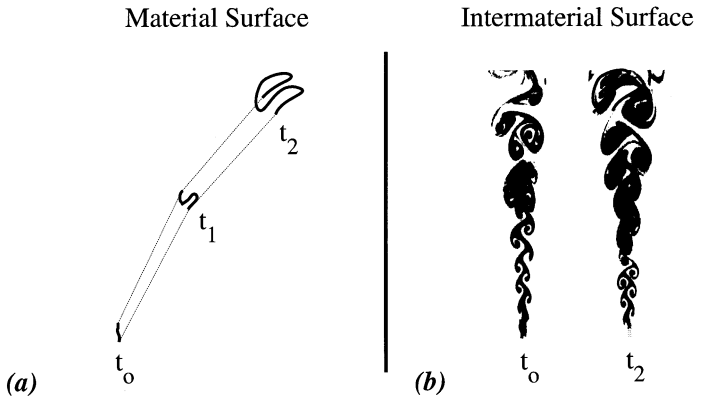

Fig. 2. (a) Example of material surface evolution. (b) Schematic of intermaterial surface evolution. Two material surfaces are selected on the interfaces at time t_0 and t_2.

any ambiguity between this and the initial definition. Finally, it is necessary to specify that, in theory, the injection of a tracer into a known flow field is a very simple concept because every particle of the tracer follows the trajectory of a massless point. In practice the integration of the material derivative (DY/Dt) in time can present problems associated with the possible chaotic evolution of the trajectories [9]. This is true too when the flow field is well defined as in laminar fields. This behavior is designated Lagrangian turbulence [20].

2.2. Reference surfaces

2.2.1. Eulerian surfaces (interface, isosurface)

When a non-diffusive tracer is introduced into part of the flow it determines an interface. This is the surface of the flow where the concentration of the tracer is discontinuous, that is where it passes from zero to a finite value on an infinitely thin surface. In other words, an interface is the place of the points in space where ∇Y_t is infinite.

Examples of interfaces are shown in Fig. 1 [21]. They are obtained by seeding the central part of a 2D plane jet by means of TiO_2 sub-micronic particles. The concentration of the particles is measured by means of elastic light scattering. White corresponds to an area in which the tracer concentration is zero. Black corresponds to an area in which the tracer concentration is equal to that fixed at injection. It is interesting to note that the tracer substance concentration in a material volume cannot, by definition, vary in time. In contrast an Eulerian, fixed, non-infinitesimal volume may contain a tracer quantity which is different according to the volume filling with the part of the flow, which has been 'traced'. If the resolution, through which the spatial dispersion of the tracer is observed, is limited, the concentration itself seems to change point by point and even the interface appears as a continuous variation of the tracer concentration. It is also possible that, in practice, the tracer concentration is so weak that its presence is hardly detectable. This happens when the tracer is transported in filamented structures so thin that its continuous distribution does not occur. Despite these experimental difficulties, the interface is a characteristic of the dispersion of one gas into another which is easily measurable, because it possesses a clearly Eulerian nature. In fact, it is possible at any time to obtain a measurement without worrying about the intricate Lagrangian evolution of the particles.

Usually the term 'stirring' is applied to the process that leads to extension and dispersion of the interface, in as much as diffusion processes are not used because stirring is purely convective.

Isosurfaces, or isolevel surfaces [22,23], are surfaces on which scalars are constant. Isobars or isotherms, which refer to pressure or temperature isosurfaces, are commonly used. On the other hand the terms isoconcentration or mass isofraction, are rarely employed. For the sake of brevity in this paper, isosurfaces will be referred to the scalar mixture fraction, Z. Isosurfaces move with respect to the fluid that transports them at a relative propagation speed $\mathbf{w}_Z$ whose orientation and direction are given by the unit vector $\mathbf{n}$, perpendicular to isosurface and oriented toward lower values of Z. Its absolute value is given by the material derivative, with respect to a reference moving with the fluid velocity, of the position of the material point (Dx/Dt), divided by its gradient ($\nabla Z = DZ/Dx$). According to this position, Gibson [23] has derived a relation which is also discussed by Pope [22]

$$|\mathbf{w}_Z| = \frac{Dx_n}{Dt} = -\frac{DZ}{Dt}\left(\frac{DZ}{Dx}\right)^{-1} = \mathscr{D}_Z\frac{\nabla^2 Z}{\nabla Z} \tag{4}$$

In fact, the material derivative of the mixture fraction, DZ/Dt, in Eq. (4) is equal to $\mathscr{D}_Z\nabla^2 Z$ for incompressible flows. A second relation between the propagation speed $\mathbf{w}_Z$ and the mixture fraction field is obtained by expliciting the gradient $\nabla Z = -\mathbf{n}|\nabla Z|$ in Eq. (4).

The divergence of the product $\mathbf{n}|\nabla Z|$ is, then, expressed

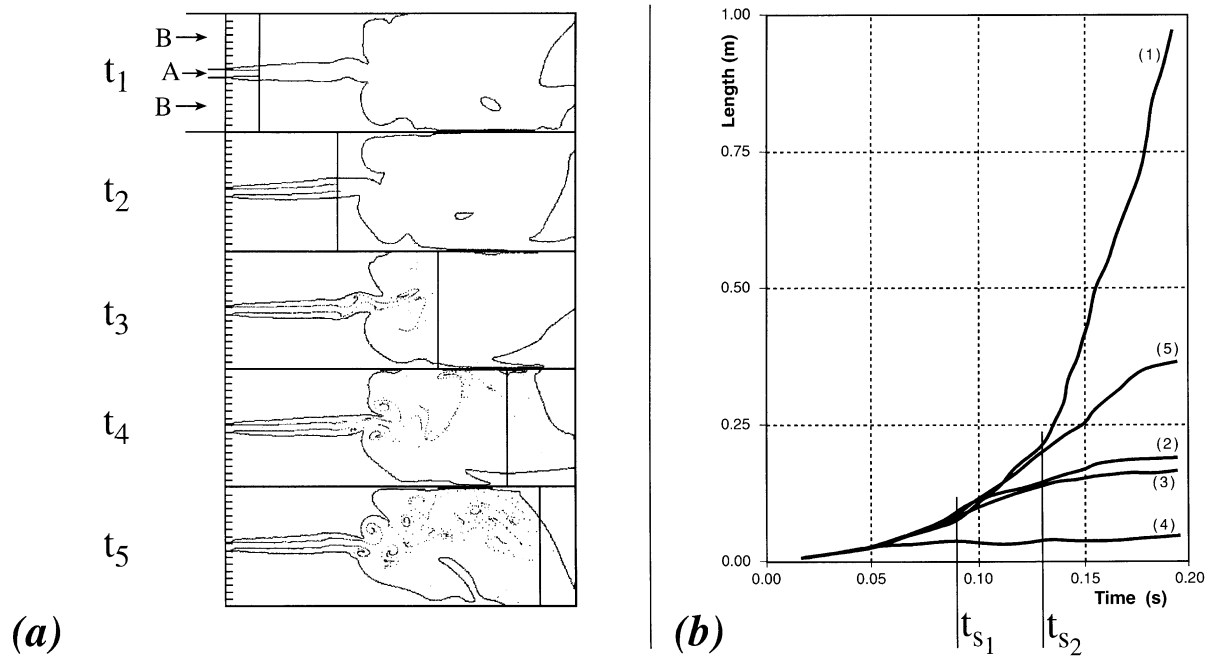

Fig. 3. (a) Sequence of progressive isosurfaces (solid contour on the left of the vertical lines) and of progressive interfaces (dotted lines). (after Cavaliere et al. [21,24]). (b) Linear extension of progressive interface (line 1) and isosurfaces (lines: 2 at $Z = 0.05$, 3 at $Z = 0.95$, 4 at $Z = 0.5$, 5 at $Z = 0.391$) section versus residence time.

according to the following equation:

$$|\mathbf{w}_Z| = \frac{\mathscr{D}_Z}{|\nabla Z|}\nabla\cdot(-\mathbf{n}|\nabla Z|) = -\frac{\mathscr{D}_Z}{|\nabla Z|}\frac{\partial}{\partial x_n}\cdot\nabla Z - \mathscr{D}_Z C \qquad (5)$$

This equation is relevant because it shows that the isosurface propagates by means of two mechanisms. The first is driven by the mixture fraction inhomogenity perpendicular to the isosurface and to its non-linear distribution. The second is related to the curvature of the isosurface, expressed by $C = \nabla\cdot\mathbf{n}$. Kinematics of isosurfaces is fully described in the papers from Pope [22] and Gibson [23], where possible discontinuity and annihilation of these surfaces are also discussed.

2.2.2. Lagrangian surfaces (material, intermaterial)

Surface is considered material when it is made up of points identified by a tracer. In other words a surface is material when it follows a material evolution [23]. Consider, for example, a 2D surface at time t_0 as it is sketched through its linear section in Fig. 2a. Every point of the surface follows a definite trajectory. At time t all these points together will make up a new surface which besides being translated and rotated is also extended or contracted. In the aforementioned figure material surfaces are sketched starting from a surface arbitrarily fixed at the point t_0. In theory a material surface cannot became discontinuous even if in practice its detection can be subject to the limits already discussed in conjunction with the interface. Surface stretching is defined as the temporary evolution of the surface area. The stretch ratio, or SR, is the ratio between the material surface area at time t and the area at time t_0, for which $\mathrm{SR} = \delta A(t)/\delta A(t_0)$.

The stretch rate $K_{\delta A}$ is the relative change of the stretch ratio, SR

$$K_{\delta A} = \frac{\mathrm{D}}{\mathrm{D}t}\ln \mathrm{SR} = \frac{1}{\delta A}\frac{\mathrm{D}\delta A}{\mathrm{D}t} \qquad (6)$$

The surface stretch rate is linked to the velocity pattern of the flow, in which it evolves, by the following kinematic relationship, fully detailed in Appendix B:

$$K_{\delta A} = \nabla\cdot\mathbf{v} - \nabla\mathbf{v} : \mathbf{nn} \qquad (7)$$

where $\mathbf{n}$ and $\mathbf{v}$ are the normal unit vector and the velocity vector of the surface δA, respectively. This expression can be read in an heuristic way as the difference between a volumetric stretch, $K_{\delta V}$, and a linear one, $K_{\delta l}$, bearing in mind that the stretch rate is additive by virtue of its logarithmic nature. The definitions of volumetric $K_{\delta V}$ and linear $K_{\delta l}$ stretch rates and their kinematic expressions are given below for completeness

$$K_{\delta V} = \frac{1}{\delta V}\frac{\mathrm{D}\delta V}{\mathrm{D}t} = \nabla\cdot\mathbf{v} \qquad (8)$$

$$K_{\delta l} = \frac{1}{\delta l}\frac{\mathrm{D}\delta l}{\mathrm{D}t} = \nabla\mathbf{v} : \mathbf{nn} \qquad (9)$$

It is also possible to demonstrate (see last part of Appendix B) that

$$K_{\delta A} = \nabla_t \cdot \mathbf{v}_t - v_n C \tag{10}$$

where $\mathbf{v}_t$ and $\mathbf{v}_n$ are the projection of the velocity vector $\mathbf{v}$ on the surface δA and the modulus of the projection $\mathbf{v}_n$ along the normal to the surface, respectively, ∇_t the divergence operator on the surface δA and C its curvature. This last expression shows that the stretch rate consists both of a contribution related to the 'planar divergence' of velocities on the surface and of a contribution related to the surface curvature.

An intermaterial surface is a material surface defined at time t_0 on the interface. In general intermaterial surfaces of practical interest are those partially limited by the first contact point (or line). By first contact point (or line) we mean the point (or line) of the interface through which the tracer passes with the shortest residence time. In a jet, for instance, the first contact line is the border of the jet's exit orifice. In fact all the possible interfaces, obtained by plotting the jet, pass through the side of the jet's orifice at residence time of practically zero. In the opposite jets the first point of contact is the stagnation point.

An example of an intermaterial line is shown in Fig. 2b. The same lines, used as example of material surface sections on the left side, are shown again together with the interfaces at time t_0 and t_2, sketched as red lines between the seeded (black) and unseeded (white) flows.

2.2.3. Eulerian–Lagrangian surfaces

Interfaces and isosurfaces are here defined 'progressive' when they refer to tracers which are injected at the in-flow boundary after a fixed reference time, t_0. They are easy to be envisaged from a conceptual viewpoint, but difficult to be evaluated by means of numerical models or experimental techniques.

In the Direct Numerical Simulation of a planar 2D flow, given in Fig. 3a, a species A, which is injected at an average velocity $\mathbf{V}_A = 1.4$ m/s into an external flow, B, which proceeds with average velocity $\mathbf{V}_B = 0.14$ m/s.

Details, concerning the flow configuration [21] and computational scheme can be found in the original article [24]. The point of interest is that at time t_0 non-diffusive massless particles are injected at the boundary in the rim which separates the two flows and they are convected downstream. The interpolating curve, shown as a solid line, determines the progressive interface at times $t_1 \ldots t_5$.

This surface is Eulerian because it is part of an Eulerian surface, i.e. an interface, and it is Lagrangian because it is bounded on one side by the tracer which is injected at time t_0 and which proceeds towards the outlet. This border line (or point, as in the 2D example) can be defined as 'leading line' (or point) at a generic residence time, t. The progressive interface always increases, with time, by definition, but the increasing rate depends on the stretch to which it is submitted. Its extension, in the example given here, is reported in Fig. 3b as a function of time with the line tagged '1'.

The progressive isosurfaces of the example reported in Fig. 3a can be approximated by the part of isosurfaces, which are upstream of the leading point of the flows, i.e. on the left side of the thick line which crosses this point perpendicularly to the main flow direction. They refer to a fixed mixture fraction, approximately corresponding to the stoichiometric value of a large paraffin–air flame, i.e. $Z = 0.05$. This is a relevant value, because it refers to a mixture fraction in the peripheral part of the mixing layer. The extension of the progressive isosurface with time is reported in Fig. 3b as line '2'. This overlaps the progressive interface up to time t_{s_1} showing that the extension of the two surfaces is identical. It then increases at a slower rate for reasons that will be clarified below. One of this consists in the fact that progressive isosurface may undergo an annihilation process when two parts of it merge into each other.

Curve '3', '4' and '5' (referred to progressive isosurface at mixture fraction $Z = 0.95$, $Z = 0.5$ and $Z = 0.38$) show similar behavior with respect to that relative to $Z = 0.05$ with different splitting time at which they separate from the progressive interface. The splitting time of the surface at $Z = 0.38$ is also marked on the abscissa with t_{s_2} because of its relevance in mixing classification, which will be presented in Section 5.

Progressive interface and isosurface are quantities, which only recently have been defined, and their experimental evaluation is not extensively documented. However, it is clear that the difficulty in their measurement lies in their Lagrangian nature. In fact, the detection feasibility of the progressive isosurface depends on the possibility of injecting non-diffusive and diffusive tracers starting from the arbitrary time t_0. This is a difficult task if the transition, from absence to presence of tracer, has to be ensured at the same time on the whole inflow boundary. Furthermore, the tracer injection at the inlet boundary can interfere with fluid-dynamic inflow conditions and it cannot be anticipated upstream of the boundary without pre-stirring or pre-mixing the traced and non-traced flows. Techniques based on smoke wire devices or on photochromic tracers, that change their physical/optical properties when crossing a light sheet on the boundary, are possible candidates to generate identifiable progressive interfaces and isosurfaces.

2.2.4. Surface evolution

The different types of surfaces defined in the previous section can be properly exploited in a framework which included all their relations both with kinematic properties, also previously defined, and with semi-empirical characteristics which can be obtained either by experimental or numerical analysis partly presented in the following.

This type of methodological approach has been first introduced by Marble and Broadwell [25] and explored in a systematic way by Candel and co-workers [26–30] in order to show the potentials of coherent flame description.

The ensemble of these works has yielded a framework which in time has given the evolution equation of the surface density which is here presented following the more formal formulation of this equation given by Pope [22] and Trouve et al. [31]

$$\sum_{Z'} = \left\langle \frac{\delta A_{Z'}}{\delta V} \right\rangle = \frac{\langle \delta A_{Z'} \rangle}{\delta V}; \qquad \langle Q \rangle_S = \frac{\langle Q \delta A_{Z'} \rangle}{\langle \delta A_{Z'} \rangle} \tag{11}$$

$$\frac{\partial \Sigma}{\partial t} + \nabla \cdot (\langle \mathbf{v}^{\mathrm{tot}} \rangle_S \Sigma_{Z'}) = \langle K^{\mathrm{tot}} \rangle_S \Sigma_{Z'} \tag{12}$$

$$\langle \mathbf{v}^{\mathrm{tot}} \rangle_S = \langle \mathbf{v} \rangle_S + \langle w\mathbf{n} \rangle_S \begin{cases} \langle \langle \mathbf{v} \rangle_S \rangle = \mathbf{v} + \langle v' \rangle_S \\ w = D \dfrac{\nabla^2 Z}{|\nabla Z|} \\ \mathbf{n} = \dfrac{\nabla Z}{|\nabla Z|} \end{cases} \tag{13}$$

$$\langle K^{\mathrm{tot}} \rangle_S = \langle K^V \rangle_S + \langle K^w \rangle_S \begin{cases} \langle K^V \rangle_{S,Z_s} = \langle \nabla \cdot \mathbf{v} - \nabla \mathbf{v} : \mathbf{nn} \rangle_{S,Z_s} \\ \langle K^w \rangle_{S,Z_s} = \langle w \nabla \cdot \mathbf{n} \rangle_{S,Z_s} \end{cases} \tag{14}$$

The surface density, $\Sigma_{Z'}$ is defined in Eq. (11) according to Pope [22] and Trouve et al. [31], as the expected ratio of surface area, $\delta A_{Z'}$, with respect to the infinitesimal volume, δV, at fixed Eulerian position, which contains $\delta_{AZ'}$. Surfaces of interest are isosurfaces, intermaterial surfaces and propagating surfaces, as premixed flame fronts. This presentation deals with the isosurfaces at fixed mixture fraction value, as it is quoted in the equation by means of the apex. A different interpretation of the isosurface density at $Z = Z'$ is given [22,31–33] in terms of the first moment of the joint probability function of mixture fraction and of its gradient, $\mathrm{pdf}(Z', \nabla Z, \mathbf{r}, t)$, or, equivalently, with respect to the module of the gradient as $\mathrm{pdf}(Z')\langle \nabla Z|_{Z=Z'} \rangle$.

The evolution equation is also reported, Eq. (12), as it has been obtained by the authors referenced before [22,31–33]. It is quite similar to any balance equation with a transport term analogous to the convective one, in which the fluid-dynamic velocity is substituted with the total velocity $\langle \mathbf{v}^{\mathrm{tot}} \rangle_S$. This is, in turn, the sum of the fluid-dynamic velocity, $\langle \mathbf{v} \rangle_S$, and the isosurface propagation velocity, $\langle w\mathbf{n} \rangle_S$. The isosurface density production is reported on the right side of the evolution equation as the product of $\Sigma_{Z'}$ itself and the stretch rate, $\langle K^{\mathrm{tot}} \rangle_S$. This quantity also consists of two contributions, i.e. the fluid-dynamic one, $\langle K^{\mathrm{V}} \rangle_S$, and that related to isosurface propagation, $\langle K^{\mathrm{w}} \rangle_S$. All the aforementioned quantities are referred to area-weighted ensemble averages and their equivalent form in terms of kinematic and scalar field variables $(\mathbf{v}, Z)$ are also reported in Eqs. (13) and (14), as they have been determined in Eqs. (4), (7) and (10). It is worth noting that the velocity is decomposed in the Reynolds averaged and the fluctuating component. The surface mean of the first is the average itself under the hypothesis of ergodicity, $\langle \mathbf{v} \rangle_S = \bar{\mathbf{v}}$, while the ensemble average of the fluctuation may be different from zero, because it is area-weighted. The evolution equation can be derived only in absence of singularities, critical points, internal edges, self-intersection (properties of surface regularity) [22]. The last property entails that annihilation process of different parts of the isosurface is not included in the equation and that an 'empirical' term should be added in order to account for this important mechanism.

The relationship between the isosurface dynamics at fixed mixture fraction value, Z', and the diffusion flame in turbulent fields is simple. In fact, the isosurface at stoichiometric condition can be considered as the skeleton of the process. The whole reaction process is concentrated in this structure, in the asymptotic limit, or part of it is centered in the reacting layer, where high-temperature oxidation takes place. The distribution of the stretch rates along the isosurface affects the oxidation rate in such a way that it determines the presence or absence of the flame and the partition of the isosurface in reacting or non-reacting components. Other elementary flame structures are related to single level isosurface. For instance triple flames are expected to propagate along this surface [34] in partially premixed turbulent flames. Similar concepts based on structure identification, are devised for premixed turbulent combustions, in terms of an evolution equation of a scalar quantity [35,36], usually named 'F' (field equation) or 'G' (G-equation). The relationship between this equation and the surface density equation is given by the aforementioned equivalence between the expected scalar gradient and the surface density. Therefore the gradient of the G-equation, multiplied, in scalar way, for the scalar gradient may be straightly related to the surface density [33]. Flame surface density models like the Coherent Flame Models (CFM) [25,32,33] are now widely used and continuously updated. Different types of surfaces may be of interest in the future, like interfaces because of their relation with the mixing. Different topological properties could be analyzed for the choice of different regimes in which the CFM have to be applied. For instance connectedness could be of interest for localizing the regions where flames could propagate starting from an ignition point.

Preliminary works have been presented, in which single terms involved in the surface equation have been modeled [37,38].

A very final comment is addressed to the emphasis given to the topic dealt in this section. This is stressed in the paper, because it exploits several kinematics quantities, which will be used along the whole presentation and therefore it shows the suitability of this approach to give a conceptual framework for the analysis of diffusion flames. Anyway it should be clear that the modeling of the quantities, as just described, is a very hard task and pose similar problems to those related to different approaches. In this sense the equivalence of the surface density with statistical moment of the joint probability density function of Z and grad(Z) or with the dissipation rate χ (presented in the following) is the

link with the approach of two variable pdf as it has been described by Meyers and Brian [39].

3. Methodological approaches

The approaches, quoted in this section, apply to any kinds of diffusive structures and they have provided the basic understanding of diffusion flames. Therefore, independently on their potentials in quantitative prediction, which are relevant too, they are of interest as conceptual guides in this field and in the formulation of more complex models. Furthermore they are pervasive in the descriptions of all the simple structures, presented in the following, and as matter of fact, they will appear in different forms several times. A reading of the fundamental works mentioned in this section, before and after reading of this paper, can give the double perspective of the whole field of diffusion flames, based on a deductive and inductive way of presentation. In particular the first parts of reviews published in this journal [40,41] are of interest in relation to any laminar diffusion flames while they address the wider field of turbulent flames.

3.1. Experimental approaches

The specificity of the experimental investigations devoted to gaseous diffusion flames is related to the capability of measuring the quantities defined in the previous section. The determination of mixture fraction and reference surfaces is particularly useful. All other measurements, such as temperature, velocity and concentration, are important both for diffusion flames and for other combustion systems, so that, they will be treated only when they are tightly related to mixture fraction or reference surfaces.

Comprehensive reviews on the measurement of scalars in turbulent diffusion flames have been presented by Stepowski [42] and by Masri et al. [43] in this journal. Measurements are necessarily based on optical diagnostics because high spatial and temporal resolutions are needed. Techniques relying on laser assisted, elastic and anelastic scattering are mainly used for this purpose. Among these, Raman measurements are mainly exploited, in studies of unconfined jet flames [44], because of their capability of simultaneous measurements of multi-species concentration and temperature.

Multi-point measurements of a single scalar quantity belong to three relevant categories of interest in gaseous diffusion flames. The first one is the measure of scalar gradient, the second one is the detection of isolevel surface with constant concentration of conserved (or material) variable and the third one is the detection of Lagrangian measurable.

The first two categories differ from each other only by the spatial domain extent. In fact the first one can be performed around different points with a limited number of highly resolved spatial sampled points, whereas the second is usually applied to wider domains with spatial integration. They can be performed in principle in 2D or 3D space. In practice they have been performed only in 1D [45] or 2D space [46] for tracer which are approximately conserved. For instance, mainly oxygenated organic compounds [47] have been used as tracers because they are capable of yielding fluorescence signals which may be related to their concentration, but, of course they cannot survive in highly oxidative zones. They are not conserved tracers in regions where fuel has been burnt. Other choices for tracers have been proposed and are under study [48] but they are related to multi-measurement techniques and therefore present some problems for their use in determining gradients or isosurfaces. It is of interest to note that the early review of Hanson on the subject of quantitative visualization [49] has not been followed by others, specific in the combustion field, in more recent times.

The third category relative to Lagrangian measurements is mentioned here for its great potentials in characterizing mixing flow, but very rare works can be quoted in it, because the measure of Lagrangian quantities is very difficult. In fact it should be performed in 3D space with aforementioned diagnostics difficulty or in very 2D case, in which the sampled material point do not leave the plane on which the measurement is performed. For instance, the intermaterial surfaces, as they have been defined before, have been measured with a limited approximation in a 2D transitional flow [24].

3.2. Theoretical approaches

The first general approach, which is mandatory to mention, attains to the description of slowly evolving diffusion field and it is related to flames in which the chemical species and the temperatures are univocally linked to the local mixture fraction. The local velocity and diffusion rates have no explicit role in determining reaction rates and flame structures are reconstructed by superposition of thermochemical variables on the mixing field. Three types of relationships between mixture fractions and these variables have been presented in several forms in the literature:

(i) temperature and composition are fixed at the stoichiometric mixture fraction and a linear mixing law is considered between this condition and the two unmixed conditions (frozen flow). The early model, proposed by Burke and Schumann [1], assumes the complete conversion of the fuel in the highest level oxidation at the stoichiometric values, with the consequent assumption of adiabatic temperature in correspondence of these values and of absence of fuel as well as partially oxidized products in the oxidizer (and vice versa). No principles restrictions prevent from assuming an other composition (for instance an equilibrium one) restricted to a single mixture fraction condition (stoichiometric or non-stoichiometric) or to other compositions (for instance determined by means of a two-steps, irreversible, infinite rate mechanism) occurring in two mixture fraction conditions [50].

(ii) equilibrium temperature and compositions are considered at each mixture fraction [6,51,52]. This assumption is based on the hypothesis that oxidation and reduction reactions can occur in the whole reacting field and they instantaneously equilibrate the reactants and products concentrations.
(iii) equilibrium temperature and composition are considered in a limited domain of the mixture fraction, where the whole oxidation activity is assumed to occur with a very fast reaction rate. Outside this range a frozen flow is hypothesized with consequent linear mixing between reactive region boundaries and unmixed conditions, analogously to the first model [53].

A second theoretical approach, which has been widely used for the analysis of premixed laminar flames [54,55], is based on activation-energy asymptotics [56,57]. It has been firstly used for the analysis of 1D diffusion flames, in which one step [5] or more than one step [58] Arrhenius reactions develop in a diffusion field. The merit of this type of analysis consists in the analytical evaluation of different flames regimes depending on the Damköhler number or on some other parameters which be a measure of diffusive–convective rates respect to reaction rates.

Finally the transformation from a coordinate system with spatial coordinates into a system including a mixture fraction coordinate has to be mentioned as autonomous significant theoretical approach [40,41,51,52,59]. The new reference system is obtained under assumption that one coordinate is perpendicular to surface at constant mixture fraction. The further assumption, that the terms, in which this coordinate appears, are of higher order respect to those depending on other coordinate in the reactive layer, allows to formulate the evolution of a reacting–diffusing field through balance equations in two variables, one spatial coordinate and the mixture fraction coordinate. The two variables can be expressed, equivalently, in terms of the mixture fraction and a new combined one, named dissipation rates of the mixture fraction [40,41,51,52,59].

A parametrization of the second variable dissipation rate is suggested in such a way that it be evaluated in a finite number of conditions either at the stoichiometric [41] or the maximum temperature location [41,50] for simplified fluid-dynamic conditions. All the thermochemical variables are thought dependent on the variable mixture fractions and on the parametrized dissipation rates in these selected representative conditions. This approach is named the flamelet approach [59] and it is of great interest since it allows to exploit data collection, also by means of simple diffusive reactive field numerical simulations, in order to generate ensemble of representative data on which statistics can be performed [60] for more complex reactive turbulent fields.

3.3. Numerical approaches

The characterization of laminar diffusion flames has received great benefit from the numerical studies on the subject [61], even though detailed kinetic schemes have been firstly developed and used in connection to premixed flames [62,63]. The computational improvement of computers as well as of numerical procedures has made possible the direct simulation of diffusing controlled structures at larger and larger Reynolds numbers with increasing level of spatial and temporal detail.

A comprehensive review of the direct numerical simulation applied to reactive flows, in the framework of more general 'model-free' simulations, is presented in this journal by Givi [64]. It is of interest to mention, according to the author of this paper, that the relation between the number of the computational cells, needed to resolve all fluid-dynamic scales, and the Reynolds number evaluated, on the length comparable with the whole domain, is proportional to $Re^{3/4}$ for each spatial dimension, at least in the considered conditions [64,65]. This entails that the number of cells is $Re^{6/4}$ for 2D structures and $Re^{9/4}$ for 3D structures. In other words a fixed number of grid points allows to resolve all the scales of 2D and 3D flows which differs from each other in the Reynolds number for three orders of magnitude. This statement is not strictly correct, because the aforementioned relationship is based on the assumption of local isotropic, homogeneous, equilibrium turbulence, which is related to 3D flows at very high Reynolds number. Nevertheless, the statement is relevant for the qualitative implication that 2D flows can be spatially resolved with much higher resolution respect to 3D flows up to a range of Reynolds number, at which transition both from laminar to turbulent regimes and from 2D to 3D flows occurs. These flows are of interest because they can be fully characterized and in the same time they present some characteristics typical of turbulent flows. In fact they are multi-scalar, but on a limited range, and they are dissipative, but on resolvable scales. This last property is responsible also of the chaotic nature of these flows, because the dissipative regions, linked in a particular way [12] through hyperbolic manifold, are the locations of positive exponential stretching of material line and surface. In other words, these regions are the locations from which trajectories of the material points with a high sensitivity to the initial conditions originate. The regimes, in which laminar deterministic Eulerian conditions and chaotic Lagrangian behaviors simultaneously occur, are also named 'weak turbulent' or 'Lagrangian turbulent' [20]. In a broad sense these flows are related to the transitional regimes and the diffusion flames stabilized in them are named transitional flames. A thorough review of this subject is given by Takeno [66] on the basis of numerical simulation.

4. Simple diffusion fields and flames

The presentation order of topics dealt with in this section is based on dimensionality of the structures. One whole section is devoted to each dimensionality. 1D structures

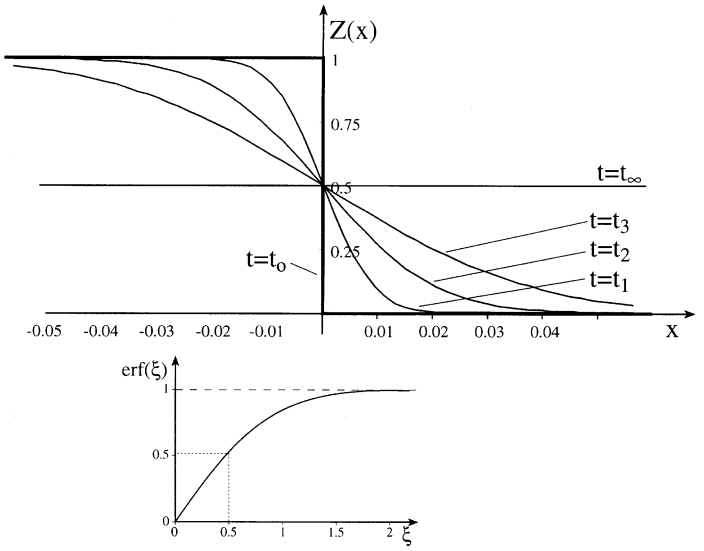

$$\frac{\partial Z}{\partial t} - \mathcal{D}\nabla^2 Z = 0$$

a) $$\frac{Z - Z_o}{Z_\infty - Z_o} = \mathrm{erf}\left(\xi = \frac{x}{\delta_m}\right)$$

b) $$\delta_m = \delta_{0.9}\sqrt{4\mathcal{D}t}$$

c) $$\mathrm{erf}(\xi) = \frac{2}{\sqrt{\pi}}\int_0^{\xi} e^{-x^2}\,dx$$

Fig. 4. 1D spatial distribution of mixture fraction according to Eqs. (a)–(c) as solution of the equation reported above. In the lower part, plot of the error function.

are, in turn, ordered according to the number of terms present in the balance equations, which describe them and 2D structures are ordered according to their level of convolution. Some particular boundaries of the paper have to be stressed. The only 1D structures considered are planar since they show with sufficient details the main fluid-dynamic influence on the diffusion flames. While the relevance of the flame curvature can be, in principle, appropriately studied in these types of structures this has not been the case of diffusion flames, in contrast with premixed flames. This is because deflagrations proceed as spherical waves from a point ignition source whereas the interest in gaseous diffusion flames has originally been generated by the use of 2D flow systems.

1D spherical–symmetric diffusion flames are dealt with in several papers when they refer to fuel droplet combustion, and specialized reviews are devoted to the topic [67] with emphasis on the specificity of the liquid presence. Nevertheless spherically symmetric gaseous flames have their autonomous interest, for the study both of curvature effect, as mentioned before, and of their relatively easy use in microgravity environment [68,69,70]. Cylindrically symmetric flames (named tubular flames) have also been studied [71].

Electromagnetic and gravitational fields have not been explicitly considered in the presentation of the structures given below. The first field yields both the electrical body forces on ions and electrons [72] in the low frequency range and the radiative fluxes in thermal heat transfer at higher frequencies [69]. The second field is responsible of buoyancy effects relevant in many 2D stabilization mechanisms [73,74] and in the vortex dynamics of diffusion flame [75,76]. The papers, quoted above in relation to these fields, can be considered useful entry-points for a thorough study of these topics.

4.1. Simple 1D plane structure

4.1.1. Unsteady, diffusive layers

A 1D unsteady diffusive layer is described by the equation

$$\frac{\partial Z}{\partial t} - \mathscr{D}\boldsymbol{\nabla}^2 Z = 0 \tag{15}$$

This is the conservation equation of the mixture fraction $_Z$ in non-reactive conditions and for constant density. If the initial condition (at $t = t_0$) is a step function (plotted as a thick line in Fig. 4) the evolution of Z can be obtained from the conventional integration of Z as fully explained in Appendix C. The integration exploits the so-called Boltzmann variable $\xi = x/\sqrt{4\mathscr{D}t}$ [77], i.e. a combination of x and t. Thus with the boundary conditions $Z(x = 0) = Z_0$ and $Z(x \to \infty) = Z_\infty$, a solution is obtained based on the error function (Eq. (a) in Fig. 4).

In the bottom part of Fig. 4 the error function plot is reported. It shows that erf(ξ) is zero for $\xi = 0$, rises linearly for values smaller than 0.6, and then it approaches asymptotically 1. It is of interest to note that, for values $\xi < 1$, the approximation erf(ξ? $\sim \xi$ is valid within a 16% inaccuracy, being erf(1) = 0.84. An approximate expression of the thickness of the incompressible diffusive isothermal layer δ_{m} is given by the value of x corresponding to $Z = 0.08$ or $Z = 0.92$. This is given by $\delta_{0.92} = \sqrt{4\mathscr{D}t}$ which is exactly the quantity by which the x variable is scaled to give the Boltzmann variable. Therefore $\xi = x/\sqrt{4\mathscr{D}t} = x/\delta_{\mathrm{m}}$ is equal to 0 at the center of the diffusive layer, and is equal to 1 in

$$u\frac{dZ}{dx} - \mathcal{D}\frac{d^2Z}{dx^2} = 0$$

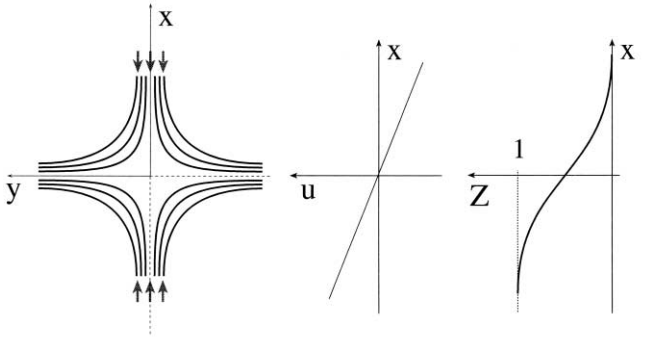

a) $-\frac{\partial u}{\partial x} = \frac{\partial v}{\partial y} = a = K_{\delta l_x} = K_{\delta l_y}$

b) $\frac{Z - Z_o}{Z_\infty - Z_o} = \mathrm{erf}\left(\xi = \frac{x}{\delta_m}\right)$

c) $\delta_m = \sqrt{4\mathcal{D}/a}$

d) $\chi \frac{\rho}{2} \frac{d^2T}{dZ^2} = 0$

e) $\chi = 2\alpha\left(\frac{dZ}{dx}\right)^2$

Fig. 5. Schematic of opposed laminar jets (left side), velocity distribution (central part) and mixture fraction distribution (central part) along the x-axis according to Eqs. (a)–(c). Eqs. (a) and (b) obtained as solutions of the equation above. Eq. (d) is the enthalpy balance under the hypothesis of Section 4.1.2 in terms of the mixture fraction dissipation rate of Eq. (e).

the marginal areas where $\mathscr{Z}$ assumes the values of $Z = 0.08$ or $Z = 0.92$. δ_m is defined as the thickness of the diffusive layer. It grows in as $\sqrt{4\mathscr{D}t}$ or it moves at speed

$$w = \sqrt{4\mathscr{D}}/2{\cdot}1/\sqrt{t} = \sqrt{\mathscr{D}/t} \tag{16}$$

To authors knowledge, there are no experimental or numerical works that describe the evolution of the reactive part of this type of diffusive layer in combustion conditions.

It is easy to presume that in the case of infinite reaction rate, the whole oxidation is concentrated on one surface, at $Z = Z_{st}$, infinitely thin and located at a distance from the reference station equal to $\delta_{Z_{st}}$. Since Z_{st} is between 0.05 and 0.08 for many paraffins [4,43] the flame is generally located on the edge of the diffusive layer. It moves further and further away from the interface, located at $Z = Z_0$ by definition.

When the reactive layer is not infinitely thin but possesses a thickness σ within the mixture fraction interval [4], it is possible to deduce a physical thickness for it, by means of derivative of Z with respect to x as reported in the following equation:

$$\frac{\mathrm{d}Z}{\mathrm{d}x} = \frac{\mathrm{d}Z}{\mathrm{d}\xi}\frac{\mathrm{d}\xi}{\mathrm{d}x} = \frac{1}{2}\frac{2}{\sqrt{\pi}}\mathrm{e}^{-(x^2/\delta_m^2)}\frac{1}{\delta_m} \tag{17}$$

This is obtained taking into account that the error function derivative is equal to the integrand of the function multiplied by the pre-exponential factor. Finally it is possible to equate the derivative of Z with the expression σ/δ_r, where δ_r is the physical thickness of the reactive layer. In the hypothesis of the linearity of Z, the derivative is in fact equal to the ratio of σ and δ_r.

Furthermore, bearing in mind that the reactive layer is on the edge of the diffusive layer, it is possible to determine the derivative of Z at a value of x equal to δ_m

$$Z = Z_{st} \Rightarrow x_{st} \cong \delta_m \tag{18}$$

$$\frac{\sigma_{\mathrm{react}}}{\delta_r} \cong \frac{\mathrm{d}Z}{\mathrm{d}x}\Big|_{st} \cong \frac{1}{\mathrm{e}\sqrt{\pi}}\frac{1}{\delta_m} \tag{19}$$

From the first equation it is determined that $\delta_r \cong 5\sigma\delta_m$, or rather that the reactive layer is equal to the thickness of the diffusive layer multiplied by five times the 'thickness of the flame' in the mixture fraction domain (σ). The σ value for fuels as methane or hydrogen has been evaluated to be less than 0.02 [4] thus δ_r is less than $\delta_m/10$. A numerical example can give some idea of the possible extension of δ_r. Let us consider the case in which the diffusive layer evolves over a time of one second and that the diffusion coefficient is $\mathscr{D} = 10^{-5}\ \mathrm{m^2 s^{-1}}$, δ_m will extend for 10^{-2} m, whilst the reactive layer (for a paraffin) would be in the order of 10^{-3} m.

4.1.2. Steady, convective, diffusive isothermal layer

A steady mixing layer can be created only if the convective transport counterbalances the natural growth of the layer. It is hard to figure out a fluid-dynamic field, which is described by the equation reported in the frame of Fig. 5. This condition is satisfied partially along the symmetry axis (or plane) of an incompressible field in which the velocity component perpendicular to the x-axis is negligible. Such field can be generated by a potential divergent stagnation flow configuration, yielded by two opposed jets, sketched in Fig. 5 by means of the streamlines (solid lines with arrows), originating from a direction parallel to the x-axis [78,79]. The velocity component parallel to the axis (u) will be given by the Eq. (a) [78] therefore it decreases along the streamlines around the symmetry axis from infinity toward the coordinate origin, around which it will be nearly negligible. From this point the streamlines diverge and are oriented

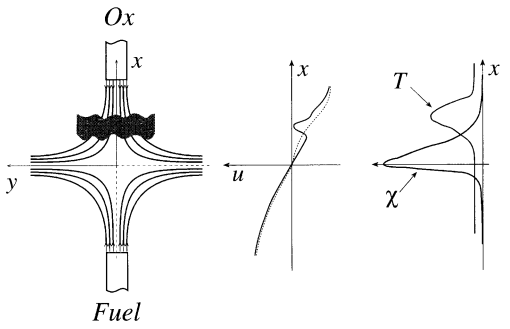

$$\frac{d(\rho u h_s)}{dx} - \frac{d}{dx}\left(\rho\alpha\frac{dh_s}{dx}\right) = -\sum \dot{\rho}_i h_i^o$$

a) $$\chi\frac{\rho}{2}\frac{d^2h_s}{dZ^2} = -\sum \dot{\rho}_i h_i^o$$

b) $$\chi = 2\alpha\left(\frac{dZ}{dx}\right)^2$$

Fig. 6. Schematic of diffusion flame (shaded area) in an opposed configuration (left side). Velocity distribution (central part) and molar fraction dissipation rate/temperature distribution (right side) along the x-axis. Enthalpy balance under the hypotheses of Section 4.1.3 is reported in the equation above and in Eq. (a) in terms of mixture fraction dissipation rate of Eq. (b).

along the y direction. Such fluid-dynamic configuration is known in the theory of dynamic system as an elliptic point to which some properties of Lagrangian non-stability are related [12]. A surface perpendicular to the symmetry axis undergoes an extension with constant stretch rate (exponential stretch ratio, according to the integration of Eq. (6)), related to a component of the strain rate usually indicated with the symbol a. The mixture fraction (Z) will be distributed similarly to the profile in the frame. It is 1 or 0 at the asymptotic boundary conditions, according to the Eq. (b), obtained as integration of the equation in the window frame. This equation is an error function of the spatial variable, x, made non-dimensional by dividing it with the mixing layer thickness. It is equal to the Z distribution in the non-steady condition with the only difference of the mixing layer thickness, which is $\sqrt{4\mathscr{D}/a}$ in this case. A typical mixing layer for bimolecular gases at room temperature and atmospheric pressure is in the order of some millimeters when the strain rate component is in the order of $10\,s^{-1}$. As it will be mentioned later, strain rates of the orders of $10^3\,s^{-1}$, to which mixing layers of the order of fractions of the millimeter corresponds, are also of interest.

It is also relevant that in this field any other conserved variable may be expressed in terms of the mixture fraction. For instance, the sensitive enthalpy (h_s) in a non-reactive field is distributed according to the following equation:

$$\frac{d}{dx}(\rho u h_s) - \frac{d}{dx}\left[\rho\alpha\frac{d}{dx}(h_s)\right] = 0 \tag{20}$$

This equation is transformed in the Eq. (d) in Fig. 5 when the spatial dependence is expressed according to the transformation $d(\cdot)/dx = d(\cdot)/dZ\ dZ/dx$ and the approximation $\rho\alpha = \text{const}$ can be posed. In the equation a new quantity, named scalar dissipation rate, χ, is defined according to the Eq. (e) in the same figure. In this term the spatial distribution of the mixture fraction and, consequently, of any other conserved variable is synthesized. When it refers to a non-uniform field, the other term, i.e. the second derivative of the enthalpy respect to the mixture fraction, must be zero. This implies that the first derivative has to be constant and, in turn, that the enthalpy or, equivalently, the temperature is linearly dependent on the mixture fraction. Such fields are also named 'frozen' and are related to such linear mixing rule.

Finally is of interest to express the scalar dissipation in the opposed jet configuration, dealt in this section, for a unity Lewis number ($\alpha = D$)

$$\chi = 2\alpha\left(\frac{1}{\sqrt{\pi}}\frac{1}{e^{\xi^2}}\sqrt{\frac{a}{4\mathscr{D}}}\right)^2 = \frac{1}{2\pi}\frac{a}{e^{2\xi^2}} \tag{21}$$

It is straight to note that there is one to one correspondence between the dissipation rate, χ and the strain rate, a. Furthermore the scalar dissipation decreases exponentially passing from the center to the periphery of the mixing layer. The ratio between the dissipation rates at the center and at layer periphery is given by $\exp(2) = 7.4$.

4.1.3. Steady, convective, diffusive reactive layer

The steady, convective, diffusive reactive layer is described by the same equation reported in Fig. 5 for conserved variable, in which the source term is added to the non-conserved one. In the case this is the sensible enthalpy, the production, given by $\Sigma\dot{\rho}_i h_i^0$ has to be added to equation in the previous section, in such a way to give the expression reported in the frame inset of Fig. 6. $\dot{\rho}_i$ and h_i^0, are the mass production rate per unit volume and the formation enthalpy of the ith species.

Mathematical formulations [5–7], numerical codes [8,53,80] and experimental measurements [2,81–83] have been used for full spatial characterization of these 1D flame structures. These works face problems (analytical, numerical and experimental) which are also found in the case of premixed flames. General procedures for dealing with these structures have been reviewed by [2,41,84,85]. The first two reviews are more related to diffusion flames than the last two.

Theoretical problems are mainly related to different levels

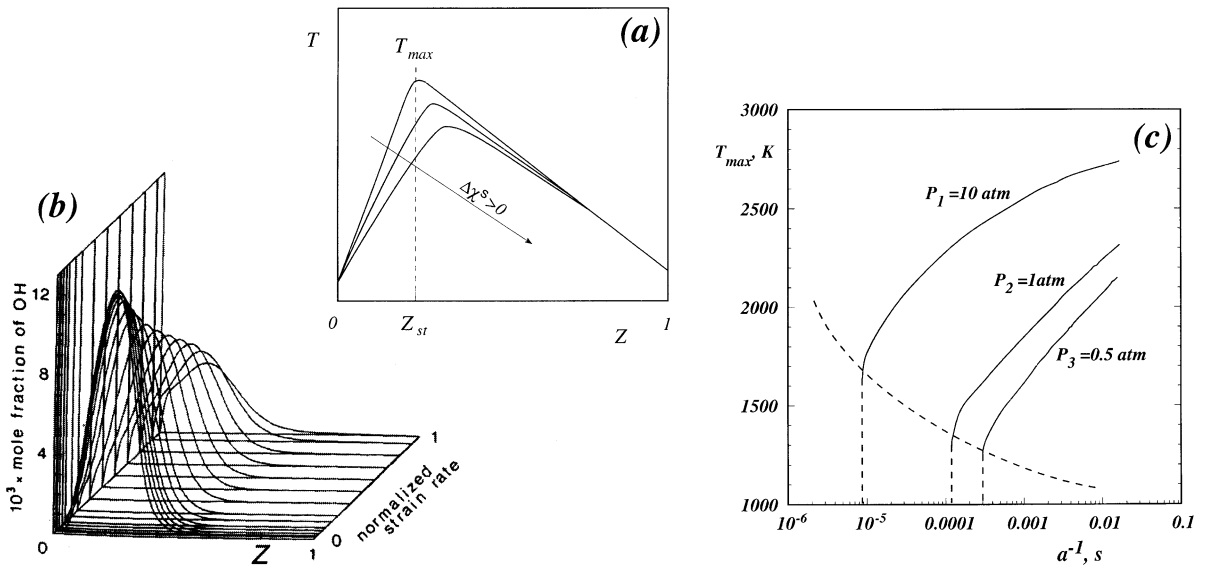

Fig. 7. (a) Example of temperature versus mixture fraction for three dissipation rates. (b) Examples of OH super-equilibrium mole fraction versus mixture fraction for different strain rates (after Dixon-Lewis et al. [91]). (c) Maximum temperature versus strain rate at different pressures for H_2/air flame (after Gutheil and Williams [92]).

of approximations and to different choices of frozen regions and of the inlet boundary conditions. Among the last ones two of them are the most common. They are either the 'potential flow conditions', for which an inlet strain rate a, or the 'plug flow condition', for which the axial component of the axial velocity gradient is neglected, are fixed. These boundary conditions are added to the other thermochemical ones [86,87]. Intermediate conditions seem to be more realistic in predicting experimental results [87] so that the other two conditions should be considered as limit case [86]. Experimental problems are not very specific of the diffusion flames (e.g. stability of the flame, spatial resolution of measure, probe interference etc.). Even though they are greater in these types of structures, because the flue-gas fluid dynamic pattern extends radially downstream of the stagnation point.

A schematic representation of the velocity and scalar distribution is given in the figure, adapted from Chelliah et al. [87] to which the reader is addressed for a full description of the reactive layer structure and for understanding the experimental, analytical and numerical origin of the profiles.

Oxygen and fuel are fed from lower and upper side, respectively. The dotted line in the intermediate part of the frame is illustrative of the velocity component (u) in the isothermal case. The presence of a diffusion flame, represented by wavy lines in the sketch, yield a positive velocity divergence, which shifts the isothermal (dotted) profile toward lower (oxidizer side) and higher values (fuel side). The mixture fraction field is represented by the scalar dissipation rate profile, because it straightway affects the heat release. The plot of this quantity, in the central part of the figure, is quasi-symmetric with a less steep and wider tail on the oxidizer side respect to that on the fuel side, i.e. at the location where temperature profile, shown in the same plot, attains its maximum. As it will be shown later, the maxima of the second derivative of the enthalpy with respect to the mixture fraction and of the heat release also occur approximately in correspondence of this point.

One merit of these structures is that the reacting field undergoes stretching in steady conditions (relatively simple experimental and modeling characterization) and that they can, in a first approximation, be described by only one parameter related to stretch. This implies an easy classification of the structures and their univocal–universal behavior for a fixed stretch value. The second property has been the subject of many studies, in which different parameters related to the stretch have been suggested to be the most representative of the whole field. The main parameters are either the strain rate ($a = |\nabla \mathbf{v}|$) or the stretch rate (K), or the scalar dissipation rate (χ) at the inlet boundary conditions and in-around the oxidation region. They are at least qualitatively equivalent, as it is suggested by their equivalence in not reacting conditions. Therefore a specific choice among these possibilities is equivalent in respect to the practical understanding of the rate control step. In contrast a widely accepted definition of the most representative parameter could be helpful in the archival storage and statistical use of databases. The velocity gradient (or strain rate) is usually chosen on periphery of reacting field on the lean side, even though some authors suggest the most invariant one to be the maximum one, located on the rich side [87]. A second, even more common, choice is the scalar dissipation rate at

the stoichiometric condition or evaluated in correspondence of the maximum temperature. The two are related, when the spatial distribution of the mixture fraction can be approximated by the frozen error function trend, reported in the previous section [41].

One use of the counter-diffusion flames is the characterization of thermochemical variables in the mixture fraction space and the behavior of the flame structure with respect to some fluid-dynamic or thermodynamic parameter.

In a first case non-equilibrium characteristics are stressed. This can be exemplified by temperature-mixture fraction plots, reported in Fig. 7a, as they have been presented in a previous review [41]. The maximum temperature is usually found on the fuel side of the mixture fraction correspondent both to the stoichiometric composition (Z_{st}) and to equilibrium maximum temperature (T_e). The curves are reported as examples relative to different scalar dissipation rates. Major species both of partial oxidation and pyrolysis are also present on the fuel side of the stoichiometric mixture fraction. For instance CO [88] (in laminar diffusion flames) and hydroxyl radicals [89–91] (in turbulent diffusion flames) for fossil fuels are detected in this composition range. This means that these species are formed in these fuel rich conditions or are diffused from the more fuel-lean regions. Examples of OH super-equilibrium concentrations are shown in Fig. 7b; lower mole fraction is reported for the condition at higher strain rate as it has been predicted in papers [89–91], by which the figure is reported [91]. The presence of other partial oxidation species like hydroperoxy radicals on the fuel side range has been predicted for H_2/O_2 systems [91].

Some other works have been mainly performed by means of the evaluation of the maximum temperature in the counter-flow diffusion flame and of its dependence on the external strain rate. A typical example of this dependence is shown in Fig. 7c, where the strain rate appears as reciprocal of the current value in order to stress the trend for high values of the strain. Each line is relative to a single external parameter and it shows its behavior for a wide domain of strain rates. The temperature variation in this range is a signature of the diffusion flame structure, which can be considered in relatively unstretched condition. For high values of a the maximum temperature decreases and it falls down at a sharp value corresponding to extinction. In fact, this way of plotting corresponds to a Damköhler number which is characteristic of the composition of fuel and oxidizer as well as of pressure and initial reactants temperature. In other words the extinction strain rate (or the equivalent extinction dissipation rate) can be considered as a state variable (dependence only on thermodynamic variables) even tough it is a fluid-dynamic quantity. Three examples of maximum temperature trends, versus strain rates, are displayed in the plot of Fig. 7c for three pressures for a H_2/air flame [92]. This system becomes more resistant to extinction as pressure increases. The dashed line in the same plot correlates the temperature and the quenching strain rates. In principle a minimum value of p can be reached beyond which no diffusion flame at all can be sustained for whatever low value of the strain rate. This can be considered a flammability limit and it is quite on the fundamental and practical levels valuable because it is accurately defined in a well-defined system. Using as parameter the oxygen mole fraction [93] this correlation has been experimentally evaluated and it yields one of the most relevant constrains in the atmospheric-pressure combustion of fossil fuels, i.e. the impossibility to stabilize a diffusion flame for oxygen molar fraction lower than 0.15 [41,93,94].

In some cases dilution of fuel either with inert [83,88] or with oxidizer [95,96] can be of interest, although these studies refer more to the first category relative to flame structure than to parametric dependence on the strain rate.

The influence of the inlet temperature has been assessed either on the strain rate [92] or on the ignition of non-premixed stream [97] (which is not considered here).

The counter-flow diffusion flames has been also exploited for many other types of studies, among which the most relevant are those relative to formation and reduction/oxidation of pollutants, like NO_x [98,99] or soot [100,101].

4.1.4. Unsteady, convective, diffusive layer

Let us consider a surface element δ_A arbitrarily chosen on an interface at the time $t = t_0$. Fig. 8 shows this element as a line $\delta l(t_0)$. The ensemble of material derivatives $\mathrm{D}Y_i/\mathrm{D}t$, at each point of $\delta l(t)$, describes the temporal evolution of δl, under the hypothesis that the tracer does not diffuse. This line (or surface) is defined as an intermaterial line. Fig. 8 also shows the trajectory of the median point (P) of $\delta l(t_0)$ in three position of δl at times t_1, t_2 and t_3.

One may introduce an orthogonal system x_n, x_{t_1}, x_{t_2} with the origin in the point P and with the x_n axis oriented orthogonally to the material line δl. In the hypothesis that the lines (or surfaces) at $Z = \text{const}$ are always parallel to the intermaterial line

$$\frac{\partial Z}{\partial x_n} \gg \frac{\partial Z}{\partial x_{t_i}} \tag{22}$$

and if the curvature of this line (or surface) in the neighborhood of the point P is small enough that surfaces at constant mass fraction are 'flat'

$$\frac{\partial^2 Z}{\partial x_n^2} \gg \frac{\partial^2 Z}{\partial x_{t_i}^2} \tag{23}$$

the balance of mixture fraction can be expressed, in terms of the x_n, x_{t_1}, x_{t_2}, and in the hypothesis that ρ and $\mathscr{D}$ are constant, as

$$\frac{\partial Z}{\partial t} + u_n \frac{\partial Z}{\partial x_n} = \mathscr{D} \frac{\partial^2 Z}{\partial x_n^2} \tag{24}$$

by expanding in series the u_n along x_n and considering only

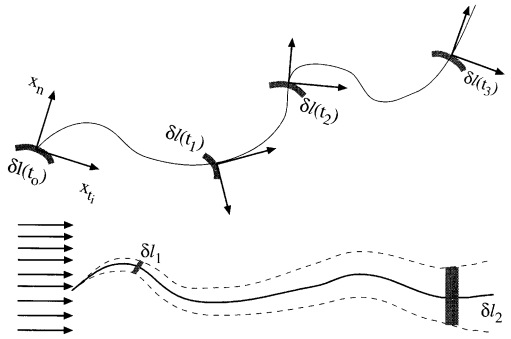

$$\frac{\partial Z}{\partial t} + u_n \frac{\partial Z}{\partial x_n} = \mathcal{D}\frac{\partial^2 Z}{\partial x_n^2}$$

a) $$\frac{Z-Z_o}{Z_\infty - Z_o} = erf\left(\frac{x}{\delta_m}\right)$$

b) $$\delta_m = \delta_m^{ns}\,\gamma$$

c) $$\gamma = \sqrt{\overline{SR^2}}\Big/SR$$

Fig. 8. Schematic of material line evolution at four times (higher part) and of mixing layer (lower part). Eq. (a) is the mixture fraction distribution, obtained by the solution of equation above, expressed in terms of mixing layer thickness (δ_m in Eq. (b)), and stretching factor (γ in Eq. (c)).

the first term

$$\frac{\partial Z}{\partial t} + \left(u_{n_0} + \frac{\partial u_n}{\partial x_n}x_n\right)\frac{\partial Z}{\partial x_n} - \mathcal{D}\frac{\partial^2 Z}{\partial x_n^2} = 0 \tag{25}$$

according to Ottino [12].

In the chosen reference system $u_{n_0} = 0$. Under hypothesis (23) $\partial u_n/\partial x_n$ can be approximated to the stretch rate of the surface, $K_{\delta A}$ In fact, the stretch rate

$$K_{\delta A} = \nabla_t \cdot \mathbf{v}_t + u_n C \tag{26}$$

can be written, under the mentioned hypothesis: $K_{\delta A} = \nabla_t \cdot \mathbf{v}_t$ and, since in incompressible and steady conditions $\nabla_t \cdot \mathbf{v}_t = -\partial u_n/\partial x_n$, it follows that the conservation equation can be written as:

$$\frac{\partial Z}{\partial t} - K_{\delta A} \cdot x_n \frac{\partial Z}{\partial x_n} - \mathcal{D}\frac{\partial^2 Z}{\partial x_n^2} = 0 \tag{27}$$

This is the governing equation for the unsteady, convective diffusive layer under the hypothesis of linear field of motion ($u = -ax$). This equation could be used to describe the evolution of a diffusive layer generated by two opposed jets (analogous to the one presented in Section 4.1.2) when the injection conditions change with time. This configuration can be hardly be realized other than imposing periodic injection conditions of the two jets (e.g. by perturbing them acoustically). Eq. (27) has been here presented by referring to a diffusive layer evolving between two parallel flows because this is a more common configuration. This situation is approximately (under the above mentioned hypotheses) described by the equation reported in the frame of Fig. 8.

The mixture fraction Z can be obtained by integrating the equation using the procedure reported in Appendix D. The evolution of Z is described by the expression a) in Fig. 8. It is formally the same obtained in the unsteady non-stretched case but, in this latter case, the diffusive layer thickness δ_m differs from the unstretched one, δ_m^{ns}, for a stretching (or squeezing) factor $\gamma = \sqrt{\overline{SR^2}}/SR$.

In principle SR and γ can be either greater or smaller than 1 but in general SR is greater than 1 and γ is lower than 1. This is the condition that controls the possibility of a true mixing of the flows. In fact, the thickness of the diffusive layer increases because of the diffusive effects, as it occurs in the unstretched case ($\delta_m^{ns} = \sqrt{4\mathcal{D}t}$), whereas the isosurface stretching around the intermaterial line reduces the mixing layer thickness. The same occurs to any structure that evolves in the mixing layer. For instance, a diffusion flame with a finite thickness, in which an oxidation reaction takes place, will be stretched in the same way of the intermaterial surface.

4.1.5. Unsteady, convective, diffusive, reactive layer

A first category of unsteady, convective, diffusive, reactive layers is described in papers which deal with analysis of spontaneous oscillations in spherically symmetric [69,102] or stagnation-flow [103,104] diffusion flames. An example of results obtained in this type of works is given by Cheatham et al. [102]. A theoretical–numerical analysis has shown that in moderate Damköhler number and oxygen concentration as well as relatively high Lewis number and heat loss the diffusion flame is susceptible to instability. This phenomenon is observed under similar conditions in microgravity candle flame.

One finds in the second category [105–112] studies in which the time-varying perturbation or boundaries conditions are imposed on a steady stretched configuration in order to analyze either steep variations or oscillations with different frequencies and amplitudes. Asymptotic or numerical models have been mainly used to analyze this case.

For instance, such initial conditions are imposed on temperature profile for a variable time that the effects, related to external addition of energy (ignition), can be analyzed [107]. Another example is shown with the help of schematic variations reported in Fig. 9a, as they have been studied in a detailed numerical analysis by Mauss et al. [108]. Stretch rates (the dissipation rate in the original

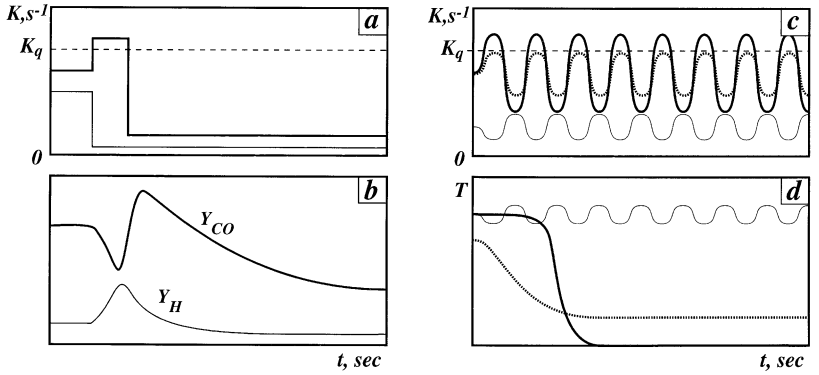

Fig. 9. (a) Three examples of steep temporal evolution of stretch rate. (b) CO and H mass fraction evolution for the case reported with thin and thick lines in (a) (adapted from Mauss et al. [108] and Barlow and Chen [109]). (c) Three examples of oscillating behavior of the stretch rate. (d) Temporal evolution of temperature for the cases reported in (c) (adapted from Ghoniem et al. [107]).

paper) approximately equal to the quenching one, but lower than it, are imposed in the diffusion flame. A small increase of the stretch value for a short period is, then, superimposed, followed by a steep decrease. The original paper analyzes different cases. For instance: (a) the increase lasts for such long period, or the decrease attains such high value, that extinction is reached in any case; (b) mild changes, in which the quenching value is exceeded for such short period or the final stretch value is sufficiently high, that only partial quenching is effective. This is the case reported in Fig. 9b, in which the maximum CO mass fraction in the flame, correspondent to the stretch variation drawn with a thick line in Fig. 9a, is reported. In this case the initial steady state value attains a new steady state value passing through a relatively fast overshoot.

Diffusion flame structure is changed also in the case a single steep decrease of the stretch rate, similar to that one reported with a thin line in Fig. 9a. In fact, Barlow et al. [109] have shown that small radicals (H, OH, O) concentrations overshoot above their steady state values relative to the new stretch rate. The thin line, reported in Fig. 9b, is a schematic example of this behavior.

Periodic strains affect the flame structure according to their amplitude as it is shown in the plots of Fig. 9c and d, which follows the analysis of Ghoniem et al. [107]. The stretch rate variation with small amplitude, reported in the figure with thin line, do not change significantly the maximum temperature and the burning rate in the diffusion flame. The temperature is shown in Fig. 9d to oscillate with the minima approximately correspondent to the stretch maxima. On the opposite side, when the stretch rate oscillates attaining values higher than the quenching steady state value (K_q), the maximum temperature, reported with thick line in Fig. 9d, decreases down to extinction values. Small amplitude oscillations can be detrimental in the sense that they depress the burning rates and lower the maximum temperature (dotted line in Fig. 9d) when they are negative even in short time of the period (dotted line in Fig. 9c). In fact in this case compression along isosurfaces correspond to separation of these surfaces as well as of isothermal surface and consequent reduction of species and temperature diffusive transport into the reaction zone has to be envisaged. The examples reported here are relative to low frequency oscillation. On the opposite, high frequency of the strain rate [107] (or equivalently of the scalar dissipation rates) may yield negligible change in the flame structure far from the quenching value or only partial extinction if the quenching value is exceeded.

Finally a separate mention is needed to the very few experimental papers present in the literature which provide information relative to internal structures [110] and to collective effects on diffusion flames. In one of these a rotating shutter is inserted in the air and fuel feeding system, which could be adjusted up to a maximum of 130 Hz [111]. The amplitude of the flame zone oscillation is shown to decrease with an increase of the frequency, according to an asymptotic first order analysis. Much higher frequency range, up to 1 kHz, has been explored by means of a speaker-driven counterflow apparatus in which velocity variations, resulted by acoustic pressure variations, have been considered dominant [112].

4.1.6. Double diffusive layer

A 1D non-steady diffusive layer has been described in Section 4.1.1 under an initial condition, consisting in a single step function of the mixture fraction *Z*. In this case such mixing layer develops that the *Z* distribution is given by an error function given by the Eq. (a) in Fig. 10.

In the case, presented here, the initial condition is the double step function drawn as a thick line in Fig. 10a. The mixture fraction is 1 in a *x*-range which extends from $x = 0$ and $x = \Delta_n$, where two intermaterial surfaces can be thought placed at the initial time t_0. The spatial–temporal evolution of *Z* follows the Eq. (a) in Fig. 10, according to the integration of the differential balance equation, as shown in Appendix A. The profiles, shown as thin lines in the Z^p–*x* plot, are

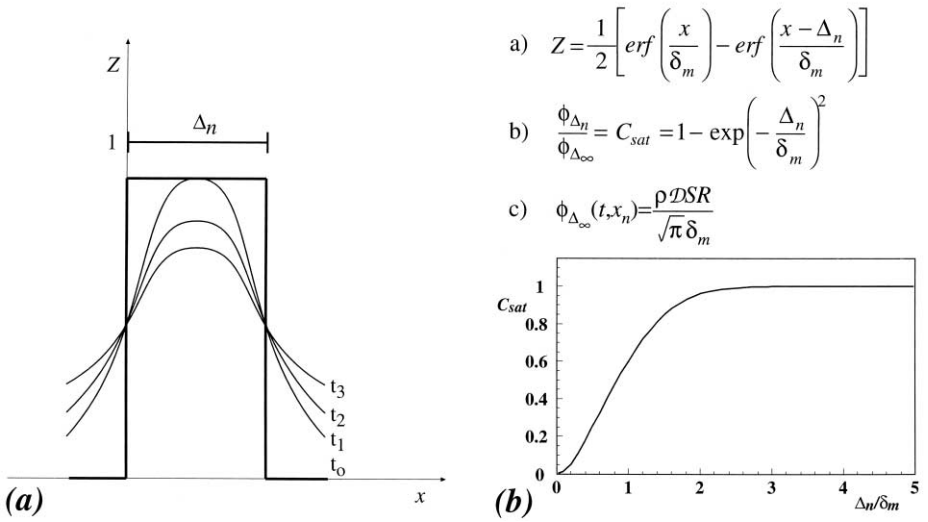

Fig. 10. (a) Example of a 1D mixture fraction distribution in a double diffusive layer at four times according to Eq. (a). (b) Saturation factor versus non-dimensional interface distance.

relative to different times, arbitrary chosen as examples. They show that the mixture fraction ranges between 0 and 1 on the beginning and then attain values lower than 1 at equidistant positions from the intermaterial surfaces.

Eq. (a) is valid also whenever the convective term is present, similarly to the case dealt with in Section 4.1.4, provided that the strain rate is the same in the whole field.

In both cases the diffusive flux through a unitary intermaterial surface at time t_0 is described in the isolated case by the expression reported in the following equation:

$$\phi_{\Delta n=\infty}(t,x=0)=-\mathrm{SR}\rho\mathscr{D}\left.\frac{\mathrm{d}Z}{\mathrm{d}x}\right|_{x=0} \tag{28}$$

where

$$\left.\frac{|\mathrm{d}Z|}{\mathrm{d}x}\right|_{x=0}=\frac{1}{\sqrt{\pi\delta_\mathrm{m}}} \tag{29}$$

In the case of a double layer, the presence of an adjacent diffusive layer can be taken into consideration by virtue of a saturation factor, C_{sat}

$$C_{\mathrm{sat}}=\frac{\phi_{\Delta_\mathrm{n}}}{\phi_{\Delta_\mathrm{n}=\infty}}=1-\mathrm{e}^{-\left(\frac{\Delta_\mathrm{n}}{\delta_\mathrm{m}}\right)^2} \tag{30}$$

This is given by the Eq. (c) in Fig. 10, as it has been derived in Appendix E following Beige et al. [113]. It can be easily evaluated from the plot on right side of figure that, when the ratio between Δ_n and δ_m is equal to 2, C_{sat} has a value of 0.95 and for a ratio value of 3, the value of C_{sat} is approximately 1. In contrast, for ratio values of 0.3 the saturation factor is already equal to 0.1. Basically:

- for $\Delta_\mathrm{n}/\delta_\mathrm{m}>2$ it is possible to consider the diffusive layer as isolated;
- for $\Delta_\mathrm{n}/\delta_\mathrm{m}<0.1$ the first diffusive layer becomes completely saturated by the second one;
- for intermediate values, the two diffusive layers interact.

It is interesting to note that $\Delta_\mathrm{n}/\delta_m=2$ corresponds to the distance at which, for paraffin/air systems, the two stoichiometric diffusive isosurfaces meet and therefore disappear, leading thus to the possible annihilation of the diffusion flame [114]. Unfortunately no experimental papers exist (at present) which describe this annihilation in 1D conditions, whereas some interesting considerations can be made on the basis of the numerical–analytical investigation of Triggvason et al. [115] for diffusion flames or for premixed methane–air flames [116]. Interactions between diffusive layers have been studied also in extinction [117] and autoignition. In this case different regimes related to mixing layers interaction has been identified, ranging from a nearly isolated behavior to that related to a nearly premixed condition.

4.2. 2D structures

4.2.1. Normal diffusion flames

In the above figure two diffusion flames are reported, which are of particular historical relevance to technology and to research. Both of them are obtained for a fuel input around the axes (or plane) of central symmetry for an extension up to r_0. Thus the mixture fraction is distributed as indicated in the two plots Z versus r in Fig. 11a and b. It is unitary at the exit of the central confinement and zero in the peripheral areas in the first case of Fig. 11a. The central flow is uniform, equal to u_0^i, and greater or equal respect to the uniform velocity of the external flow (u_0^e).

Here only a brief and simplified treatment of the subject is

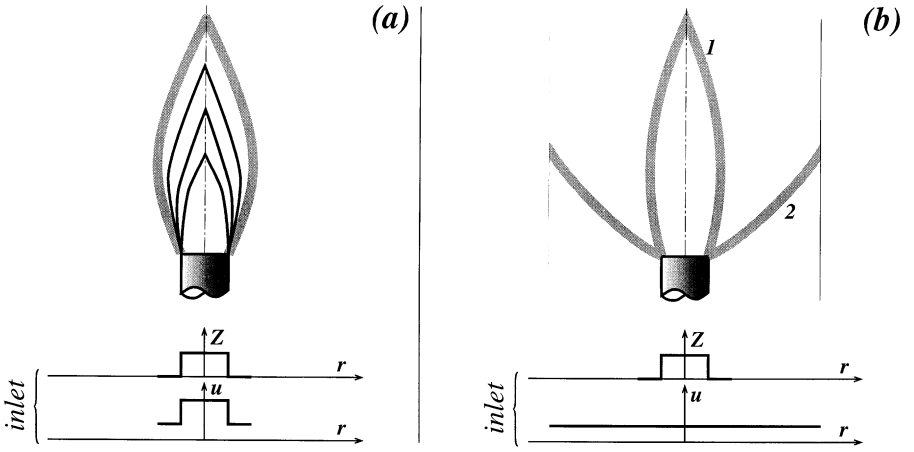

Fig. 11. Schematic of laminar diffusion flame. The shaded area represents the reacting zone: (a) jet-like diffusion flame; (b) Burke and Schumann diffusion flames in over-ventilated (1) and under-ventilated (2) conditions.

undertaken giving the idea of a first approximation of the behavior of these structures. For a full treatment of the subject, many books may be consulted, for instance Kuo [14]. It is interesting to stress that these structures can also be subject to a far more detailed descriptions with the aid of realistic numerical models as it has been shown in the numerical–experimental comparison in an aforementioned paper [61]. Both flames are not in themselves structures of particular interest in turbulent flames and thus the classical consideration, here reported, would seem to be sufficient in order to capture their essence. In both cases, based on the hypothesis of steady state, no buoyancy effects, complete isobaricity, constant density and $Pr = Le = Sc = 1$ the conservation equation of momentum, or mixture fraction, are similar and analytically resolvable. In the first case, the solution obtained by Spalding [118] and Schlichting [119] presents isosurfaces such as the one reported in Fig. 11a. One of these isosurfaces (at $Z = Z_{st}$) under the further hypothesis of infinite reaction rate, represents the area where heat is released (shaded line) in attached diffusion flames.

It is also possible to demonstrate that velocity along the axes, u_c, where the subscript c stands for central line, or the mixture fraction along the axes Z_c can be expressed in the far field as

$$\frac{u_c}{u_0^i} = \frac{Z_c}{Z_0} = \frac{1}{x}\left(\frac{3}{4} l_z\right) = \frac{1}{x}\left[\frac{3}{4}\left(\frac{1}{2} v u_0^{i^2} r_0^2\right)\right] \tag{31}$$

when the external velocity is negligible. Apart from the constants l_u and l_z and the kinematic viscosity v all the other quantities have been defined.

Axial velocity and mixture fraction, u_c and Z_c, diminish as $1/x$ along the axis outside the singular boundary condition.

The hypotheses mentioned above can be left aside in order to give a more realistic description of both the numerical model and the analytical treatment. For example it is possible to neglect the hypothesis of $Sc = 1$ and obtain the ratio between the flow field and the mixing composition as: $Z/Z_c = (U/U_c)^{Sc}$.

It is interesting to note that the mixture fraction can be obtained from any conserved variable β like Schwab–Zel'dovich variables obtained from linear combinations of mass fraction of fuel and oxidizer with constant proportionality equal to stoichiometric coefficients.

The second case, described in the scheme reported in Fig. 11b, is the one treated by Burke and Schumann [1]. In this case, the whole system is confined, the fuel and oxidizer velocity are equal. By varying the ratio of the inlet areas one changes the ratio between their flow rates. If the ratio is greater than the stoichiometric one the flame reduces on the axes (case 1). They refer to this flame as 'over-ventilated'. If the ratio is lower than the stoichiometric value the flame opens and extends intersecting the external confinement (case 2), the flame is referred to as 'underventilated'. Other uses of these types of structures are in partially premixed flames [120] and in the pollutant formation, in particular for carbonaceous particulate and PAH [121,122] due to the wide pyrolitic region present on the rich side of the flames. These topics are not dealt here, as it has been anticipated in the introduction.

4.2.2. 'Reverse' and 'inverse' diffusion flames

In the flow configuration, of Fig. 12a, the fuel velocity is lower than that of the external oxidizer flow. On the basis of the velocity ratio, the distribution of the mixture fractions can be similar to that of the first jet configuration analyzed in the previous section or can be closer to that yielded by a wake with two vortices counter-rotating around their axes. In general there is an inward reverse flow, which can be steady and symmetrical or can be unsteady similar to the periodic Kármán vortex street [123], occurring in a wake. Flows in the first category are unstable, and not often considered in combustion. For instance one half of this

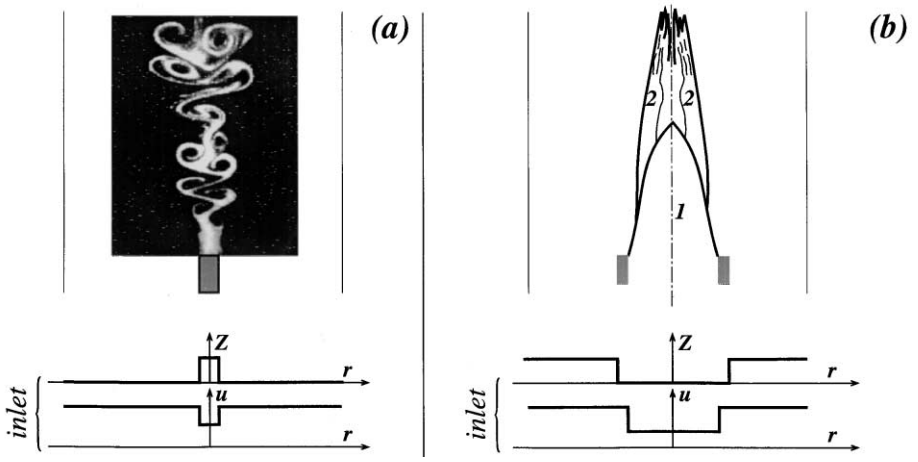

Fig. 12. (a) Interface of isothermal flow in 'reverse' flame condition. (b) Schematic 'inverse' flame (after Wu et al. [132]). 1: blue emission zone; 2: orange emission zone.

flow can be well represented by a wall flow which undergoes separation in presence of a bluff body. Some authors have exploited this configuration in reactive conditions [124] in order to analyze the increase of heat transfer into the fuel. In contrast, flows of the second type are widely described in the literature, at least in isothermal conditions [125].

An example is shown in Fig. 12a. It is relative to a 2D planar flow adjusted to a velocity ratio of 1.75 and a velocity of the internal flow of 0.4 m/s. The white color marks the regions where elastically scattered light from tracer particles, injected in the central flow, is detectable [126]. The boundary with the black region is the interface, as it has been mentioned before. The alternate shedding of vortices on the left and on the right side is observable. The main characteristic is that fuel strips, represented in white color, are embedded inside a vortical structure of the oxidizer flow. In turn this reverse flow has to be included, as structure, in the category of single or multiple vortices, which will be considered later.

Many other 2D fluid-dynamic structures with centerline recirculation zones have been studied for combustion applications due to their beneficial effects on flame stabilization, but they generally refer to turbulent regimes and will not be considered in this review. Configurations with regions of inward reverse flows can be obtained also by opposed jet [127] or swirling flows but their relevance is linked to the possibility of substaining flames with high velocity inlet conditions. Interest in swirled flows is testified by the wide literature on the topic and by the fact that this category of flows is dealt in several books [128,129]. The same comment applies for other flows like submerged [125] and sudden expansion jets [130] in which outward flow structures are present. In fact, they are analyzed in relation to turbulent regimes, even though their similarity to simple laminar structures can be of interest in envisaging possible links and analogies. A broad-ranging review, which covers both aspects of laminar and turbulent regimes, is given by Edelman and Harsha [131].

A diffusion flame is defined 'inverse', when the oxidizer and fuel streams are inverted respect to the 'normal' diffusion flames. In concentric coaxial flows the oxidizer is in the central part of the flame and the fuel is outside. The sketch Fig. 12b shows the inverse diffusion flame, as described by Wu and Essenhigh [132]. The profile of the mixture fraction Z attains unity (only fuel) in correspondence of a double plateau, which represents the annular fuel stream. In this configuration oxidizer ($Z = 0$) is present around the central symmetry axis.

While this configuration has been used in practical burners and seems to produce less soot than normal ones [133] only few papers deal with fundamental aspects and with measured characteristics. Among these it is worth mentioning a classification of such flames in terms of their structures [132]. Six major regimes are identified with the common feature of blue emission region, which encloses the central part of the flame (zone 1 in Fig. 12b). Orange emission region (zone 2) may be present in an annular region around the blue one. It is notably that the inverse underventilated flames are not luminous and that the flame surface profiles of the normal and inverse flames are mirror image of each other. The flame tip is also analyzed in terms of temperature and species distribution, but the results provided do not suffice in order to gain a clear conceptual framework in which the annihilation of two laminar diffusion flames on the oxidizer side can be categorized.

4.2.3. Triple flames

The triple or tribrachial flame is a structure which has characteristics of premixed and diffusion flames. A triple flame can be produced in a medium in which the mixture fraction is not uniformly distributed and when the ignition occurs around $Z = Z_{st}$ or in the case of external input of

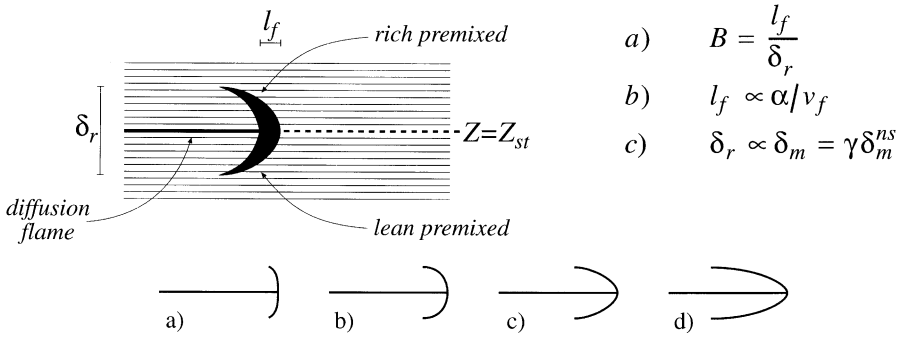

Fig. 13. Schematic of triple flames. Eqs. (a)–(c) stand for stratification parameter, laminar premixed flame thickness and reactive layer thickness. Sketches a–d are schematic of triple flames according to the stratification parameter B.

ignition energy or in the case of compression heating. Another example of triple flame is the structure that guarantees the stabilization in high strain rate of jet outlet of a lifted laminar diffusion flame. A 2D scheme, which sums up the aforementioned structure, is shown in Fig. 13. The thin lines represent the isosurfaces at different values of mixture fraction Z. The dashed line is the isosurface relative to a stoichiometric Z. On such a distribution of Z it is possible to set up a flame, which is represented in the frame by the arrow-shaped dark region. In this part of space heat is released due to oxidation of fuel ignited through various mechanisms that will be discussed later.

In the triple point situated in the apex of the flame, on the stoichiometric isosurface, combustion propagates as in a premixed flame. In the frame this occurs towards the right, or rather towards the mixing region where the mixture has not yet reacted. The flame front curves in the rich and lean regions, because in these conditions the laminar flame propagation is always lower than that obtained along the isosurface corresponding to the stoichiometric air–fuel molar fraction. This curved premixed flame leaves behind, in its passage (to the left of the curved zone in the frame), two regions in which there will be a residue of fuel or oxidant, in the regions at lean and rich conditions, respectively. Thus along the stoichiometric isosurface, a diffusion flame sets itself up completing the reaction of the fuel or oxidant exuberantly with respect to the stoichiometric (value). In the lower part of the frame, four schemes of triple flames are reported. The first from the left shows that the branch relative to premixed flames is fairly flat. This condition occurs when the mixture is virtually homogeneous and thus the isosurfaces are spaced very far away from each other. On the extreme right a very curved premixed branch is represented, practically parallel to the diffusive branch. In these conditions the Z gradient around Z_{st} is very steep. In order to quantitatively justify the regimes, in which triple flames occur with different degrees of curvature of the premixed branch, the stratification parameter or Dold number, B, is used [134,135].

This is the ratio between the thickness l_f of the premixed flame (in stoichiometric and non-stretched conditions) and the 'reacting' thickness δ_r inside the diffusive mixing layer. The first quantity is dependent only on the composition and on the thermodynamic initial conditions of the mixture and it is a measure of the average reaction rate. The second quantity depends on the fluid-dynamic evolution of the mixture and takes into consideration its stratification. It is proportional to the mixing layer thickness δ_m, which, in turn, is in proportion with $\delta_m^{ns} = \sqrt{4\alpha t}$ multiplied by a stretching (or squeezing) factor γ equal to $\sqrt{\overline{SR^2}}/SR$, as it has been presented in Section 4.1.4. This is also in proportion with the dissipation rate $\chi = 2\alpha(\nabla Z)^2$. For B equal to zero, the nearly flat premixed branch structure, previously described is obtained. The velocity of propagation of the flame is positive and higher than that in homogeneous combustion field. For B approximately equal to 1, the curvature and the area of the diffusion flame are of the same order of magnitude (second scheme on the right hand side of the frame). As B increases, two notable values are obtained, B_0 and B_q. In correspondence with the former, the flame propagation speed becomes negative, whereas $B = B_q$ leads to the extinction of the triple flame.

The literature regarding the triple flames is relatively recent and is largely analytical and numerical [136–140] whilst only a few experimental studies and comparison with models has been undertaken on this subject [141,142].

The role of this structure is also relevant in rim bounded Navier–Stokes, triple-deck region [141–144] for which adiabatic or non-adiabatic conditions and local stratification parameter determine the location of the structure in respect to the boundary.

The characteristics of triple flames have been also related to anomalous behaviors in terms of Lewis [136,145] and Schimdt [141] numbers.

4.2.4. Single vortices

The kinematic evolution of an interface can be schematically portrayed as a sequence of the frames, illustrated in Fig. 14 from (a) to (d). In the first frame the roll-up of the protuberance that evolves from the flow, represented in black, is shown accompanied by a curvature of the diffusive

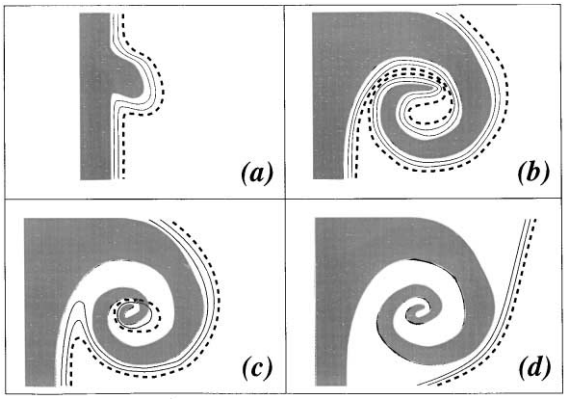

Fig. 14. Example of interface (contour between shaded/non-shaded areas) and isosurface (thin lines) sequence showing a single vortex convolution. Dotted lines represent the isosurface at stoichiometric conditions.

layer too. In fact both generic isosurfaces, represented by the continuous lines, and the isosurface corresponding to the stoichiometric mixture fraction, represented here by the dashed line, follow the interface (contour line between black and white regions) in a parallel way. This behavior makes reasonable to describe this diffusive layer through the 1D, unsteady, stretched layer, dealt in Section 4.1.5. In reality, with respect to this simplified model, different factors come into play. Some of these are here reported in an ordered list according to their relevance:

(i) interaction between contiguous diffusive mixing layers;
(ii) distribution of the stretching along the stoichiometric isosurface;
(iii) expansion of gases due to heat release and consequent induced stretch distribution;
(iv) curvature of isosurfaces.

All these factors are effective in different ways according to the initial conditions of the evolution of the vortex or, in other words, according to the thickness of the diffusive layer at the moment when folding begins.

The flame/vortex interaction has been reviewed by Renard et al. [146]. This is a very exhaustive review ranging from the very first works on the subject [147], including the DNS calculation [148], to the more mature achievements in the numerical [149,150] as well as experimental works [151]. Ashurst and Williams [150] have analyzed some of these elements in qualitative terms by means of a numerical simulation. The hypothetical schematic description presented in the four frames above is based on their work. The authors demonstrated two important features that can be highlighted in a comparison of frames (b) and (c). The first is that isosurfaces become disconnected and form islands (see frame c), due to the annihilation of different parts of the same isosurface. The second is that inside the spiral structure, individuated by the interface, it is possible for the isosurfaces to undergo a rarefaction and form peninsulas due to the compression along the isosurfaces in correspondence with the vertexes of this peninsula. This evolution of the vortex leads to the expulsion of many isosurfaces outside the spiral form structures and eventually the situation set out in frame (d). It seems that such a situation is favored by the heat release location with respect to the vorticity distribution [152].

To be more specific, it is of interest to mention that the spatial distribution of these quantities has been shown to be effective in yielding interface-flame separation for the near field of a 2D, planar diffusion flame by Soteriou [153]. The distribution is such that the mixture fraction region, where the exothermic reaction occurs, and the region with the highest vorticity level may be separated just downstream of the nozzle rim due to the wake-modified velocity distribution at the inlet boundary. Furthermore the positive velocity divergence due to volumetric expansion of the exothermic-reacting regions can both push the flame further away from the vorticity zone and depress the vorticity level in the reaction regions, which in turn means less flame-surface folding. In synthesis it is conceptually relevant to identify two classes of mechanism, which separate the interface from isosurfaces mixture fraction. The first is the one just described, which will be referred in the following as 'splitting mechanism', whilst the second is the aforementioned 'annihilation' process.

In the last case it is also true that if the vortex which generated the rolling of the interface is still active, the stretching rate of the stoichiometric isosurface can generate stretching or compression of the isosurface itself.

Katta and Roquemore [154] have shown that if the vortex is on the fuel side (as is generally the case in vortices generated in shear layers) at the center of the vortices, the isosurfaces undergo stretching with an increase of the local temperature. The opposite effect occurs when the vortex is on the oxidizer side such as those generated by the buoyancy.

4.2.5. Vortex couples

2D vortex couples are of different types: counter-rotating (as illustrated in Fig. 15a and b) and co-rotating (as shown in frames c and d). The interest in the former lies in the possibility of creating experimentally the impulses which generate them in well defined laminar flow fields. These structures have been used in several experiments and have given rise to two types of studies. These are related to pulsed fuel jets (frame a) or to travelling vortices both inside the fuel (frame b) or inside the oxidizer flow. In case (a) the interface (which borders onto the black area) is a spiral-form structure and the diffusion flame, represented by the dashed line, in correspondence with the stoichiometric isosurface follows the dynamics of the interface. From the early work of Karagozian and Marble [155] to the more recent investigations

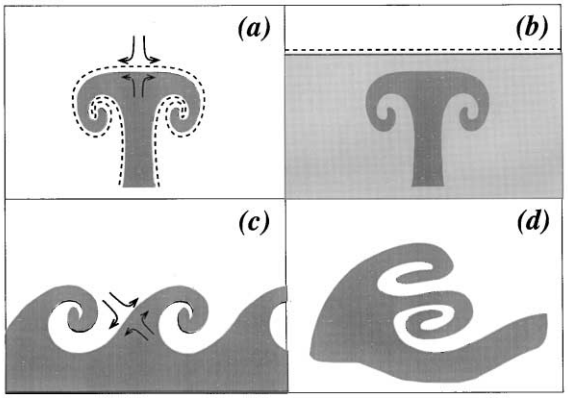

Fig. 15. Vortex couples examples: (a) counter rotating vortices at interface; (b) counter rotating vortices far from interface; (c) co-rotating vortices; (d) co-rotating vortices merging.

under microgravity condition [156] the evolution of such a spiral structure can be captured. The area inside the vortex is occupied by the oxidative activity and by products of combustion, present also in the form of several islands inside the vortex head. The case described in (b) differs from (a) as there is an initial time interval in which the diffusion flame is affected by the presence of the vortex only in terms of stretching. Takahashi and Katta [157], by means of a numerical simulation, brought into evidence that this stretching leads to the thinning of the diffusive structure with a consequent loss of reactants which cross the flame and an increase of flame cooling. Other experimental studies [158,159] (extended to comparison with numerical simulations in the case of the former paper [157]) indicate that the whole diffusion flame, crossing an intense vortex, can extinguish or that a part of it may be quenched for a short period after which the whole flame structure can be rebuilt.

It is worth noting that the vortex couple, unlike the single vortex, presents a strong tendency to extinguishing the diffusion flame. This is due to the presence at the apex of the structure, between the two spiral-form zones, of an area in which stretching is more intense. In fact, in this zone as seen in Fig. 15a), the flow field is typical of a stagnation point. A deeper insight [151], by means of experimental/numerical comparison of the data, has shown that annular quenching, away from the stagnation point, may prevail when the oxidizer side vortex is forced to cross the diffusion flames at moderate speed. This quenching, referred to H_2/air system, occurs at equal or lower strain rates than that at the stagnation point and it is due to combined effects of selective molecular diffusion and curvature. Particular temporal and spatial correlation have been studied under flame vortex–flame interaction conditions, in terms of minimum time required for quenching [160] as well as for increasing the flame surface [161].

The common characteristics between the vortex rings of Fig. 15a and b and the co-rotating vortices sketched in Fig. 15c is that the interfaced area of greatest extensional stretching is in the braids between vortices [162], whilst the spiral structures tend to roll up with an almost rigid rotation. Anyway the possible presence of compressive stretching along the diffusion flame surface has to be underlined, because it produces an increase of the reacting layer thickness [163].

A structure, consisting in only two co-rotating, vortices, sketched in Fig. 15c) (unlike the case of contra-rotating vortices) is not easily created experimentally but it occurs in mixing layers of ‘transitional’ jets as well as in numerical studies [164,165]. Generally the evolution of this structure is a growth with multi-spires or also a coupling with the vortex which precedes or follows it. The vortex couples can in turn be squeezed or refolded as if they were single structures. It is clear that this process, affecting one (or more than one) vortex, leads to the nearing of the interface and consequently to the acceleration of the annihilation process of the isosurfaces. It is plausible to suppose that in this case too, as with the single vortex, the evolution of the vortex will lead to the expulsion of the diffusion flame from the central zone of the spirals.

Very few papers have been devoted to the dynamics of more than two vortices, even though the aforementioned one [164] shows similarities with the case of only two vortical structures in the possible occurrence of pairing and merging mechanisms.

4.3. 3D structures

This section is devoted to outline some possible effects related to diffusion flames in simple 3D structures. The literature in this field is very poor and the only papers, which deserve a mention, are quoted here only for their analogic implications and for the descriptions of part of the effects involved in the whole process. Therefore the following statements are conjectures and not observed facts. They are presented only for lust of completing a

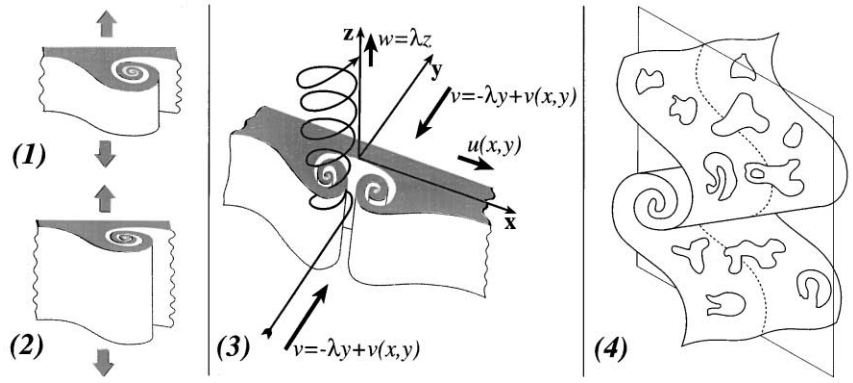

Fig. 16. (1) and (2) Schematic of vortex stretching. (3) 3D steady-state vortex. (4) Schematic of 3D isosurface. Dotted lines stand for the intersection of isosurface with an arbitrary plane.

pictorial visualization of the diffusive structure and may be useful as possible orientation of the research work.

A well-known 3D effect, related to isothermal fluid-dynamic, is the stretching of a vortical structure [165,166]. This is depicted in Fig. 16(1) and (2). An interface is sketched as surface separating a black region (say seeded by a tracer) from a white one (say not seeded region). A fluid-dynamic pattern is thought to yield both vorticity and linear stretch rate parallelly aligned to the arrows [167]. In this peculiar case the positive stretch along the arrows yields a negative one perpendicularly to the interface, i.e. a nearing of different parts of the convoluted interface. The vortical structure depicted in Fig. 16(1) deforms in the stretched omeomorphic structure sketched in Fig. 16(2). The implication in a diffusive field is that the isosurfaces distances also become squeezed. In the case a whole mixing layer develops along the interface, both its thickness (δ_m) and the distance between the interface (Δ_n) decrease according to the intensity of the stretch rate. The ratio of these two lengths should be constant in presence of an uniform stretch field, therefore the saturation ratio, defined in Section 4.1.6, should also be constant with a consequent negligible effect on the mass diffusion flux through the interface. In other words it is plausible that the fluid-dynamic pattern associated to this structure counterbalances the tendency of isosurface annihilation, even in presence of the flux enhancement due to stretch influence on the isolated layer.

A second 3D structure is presented in Fig. 16(3). In this case the interface is folded by two counter rotating vortices, which are fed by a uniform velocity stream coming along the y-axis. A characteristic trajectory, drawn in the figure by a solid line, shows an undisturbed part at infinity, whereas it follows a spiral path inside interface convolution. The analytical dependence of the three velocity components on spatial co-ordinates is reported in correspondence of the full arrows. It is such that stretch is effective only in the plane y–z, whereas the not deforming convolution is active only in the x–y plane or, in other words, the vorticity is aligned on the z-direction, parallel to the stretch. This characteristic is common to the stretched vortical structure described before. The main difference between the two is the steadiness and the periodic distribution of vorticity of the second structure. A full analysis of this topic is given by Dold [167,168] in relation to isothermal and premixed regimes. It deserves mention due to its uniqueness and to some peculiar phenomena related to it. For instance, a flame trapping mechanism is identified, in fact a laminar flame propagation originated along the x-axis may undergo a convective preferential transport inside the vortex core where it is more resistant to the quenching. The diffusive regime has also been studied inside this structure [169] and it is still object of active research.

A third feature related to 3D diffusion flame is outlined with the help of sketch 4. This represents an isosurface, which extends in a 3D domain and it includes some 2D discontinuities on its surface. The dashed line, which is the intersection between the isosurface and a plane, is also discontinuous because itself intersects the 2D discontinuities, but it differs from this because it cannot keep connection. This is another main difference between the 2D and 3D structures of diffusion flames. The first one looses the connection if 2D annihilation of some part of the isosurface occurs, whereas the second one may be annihilated in some regions, but it keeps its connection degree.

It has to be stressed again that the considerations presented here are basically speculative and they want to be only suggestive. A start reading for a deeper research in this field are the papers dealing with the identification [165] and analysis [167] of 3D isothermal structures.

5. Evolution of simple structures, their group behavior and classification of regimes

5.1. 2D quiescent plane systems

A random distribution of the mixture fraction in quiescent conditions can be obtained by injecting fuel into a turbulent

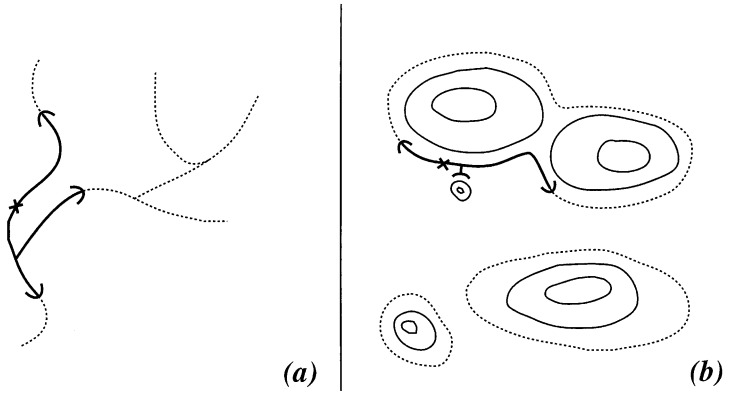

Fig. 17. Sketches of non-steady triple flame propagation along open (a) and closed (b) isosurfaces. Dotted lines stand for stoichiometric surface. Solid line marks burned/burning region. The crosses are the ignition points.

flow field or into a laminar flow field with chaotic-Langrangian characteristics. After the arrest of the flow field a random composition distribution is obtained which is also know as 'fossil' turbulence [170,171] and it is in fact the residue of the real turbulence. This non-uniform composition is interesting in the case of combustion because, as with the contra-diffusion 1D flames, it is above all the distribution of the mixture fraction gradient ∇Z which regulates heat release. When ∇Z (or the scalar dissipation rate, χ, or the stratification parameter, B) is very low the flame is approximately in chemical equilibrium, whereas when ∇Z (or χ or B) is very high, the flame tends to extinguish or not to ignite. In examples of Fig. 17a and b it is thought that ignition comes about at the points marked with crosses and that triple flames originate here. Autoignition either occurs (for instance when there is a compression heating in diesel combustion engine) if temperatures exceed a predetermined threshold (and of course if ∇Z or χ or B are low enough), or through external input of other energy forms (for instance in spark-ignited engine). After a period of transition dominated by a explosive evolution of the early kernel [138], triple flames travel along the stoichiometric isosurfaces (indicated by dashed lines in the fresh mixture and by solid lines in the burnt mixtures). In Fig. 17a these surface are all connected, hence, from the bifurcation, branches sprout out along which triple flames travel with their characteristic mushroom shapes, represented by curved black lines at the dashed line border, i.e. in the areas where heat is released in a deflagrative propagating mode. If the isosurfaces are not connected, like in Fig. 17b, the triple flame structure can be observed only in the areas where stoichiometric isosurfaces are connected to ignition zone. It is plausible to suppose that, if the triple flame originates close to isosurfaces that are within the limits of inflammability, an arch-shaped front could be formed such as those traced in Fig. 17 or in Fig. 13. If this is not the case and the ignition takes place, in the flammability limits, out from the isosurface in stoichiometric conditions the flame propagation is still anisotropic, but the residual diffusive–reactive structure is created only after the flame reach this stoichiometric isosurface.

This simple schematic example is based on the concepts presented by Domingo and Vervish [138] for a quiescent and 'turbulent' 2D non-uniform mixture fraction distribution. The description of the reactive field is obtained by numerical model with single step kinetic rate when auto-igniting conditions are reached by means of compression. The main difference respect to this oversimplified description consists in the extension and location of the ignition. In the last case ignition is related to stoichiometric isosurfaces and it extends along these surfaces in the regions where ∇Z or χ or B do not exceed quenching values. If these quantities are very low, autoignition takes place on the whole stoichiometric surface, then two premixed flames propagate toward the rich and the lean side, while a diffusion flame is centred on the stoichiometric surface.

Further refinements can be taken into account, like the proper air–fuel ratio condition for which the fastest auto-ignition delay is obtained or like the possible occurrence of consecutive autoignition processes at different mixture fraction values. That is a condition similar to the one in which the deflagrative-detonation transition may occur too [172], but the main picture will not change substantially.

Between the two extreme conditions of single point ignition and of the whole surface autoignition, intermediate conditions are reported [138] in which the initial explosive deflagrative structures is limited to a restricted zone and it develops into triple flames, yielding a double peak in the temporal heat release profile.

5.2. Simple 2D flow systems

5.2.1. 2D flow systems

2D flow systems are suitable to study complex mixing fields in isothermal and reactive conditions. In fact random characteristics either of spatial distribution of scalar

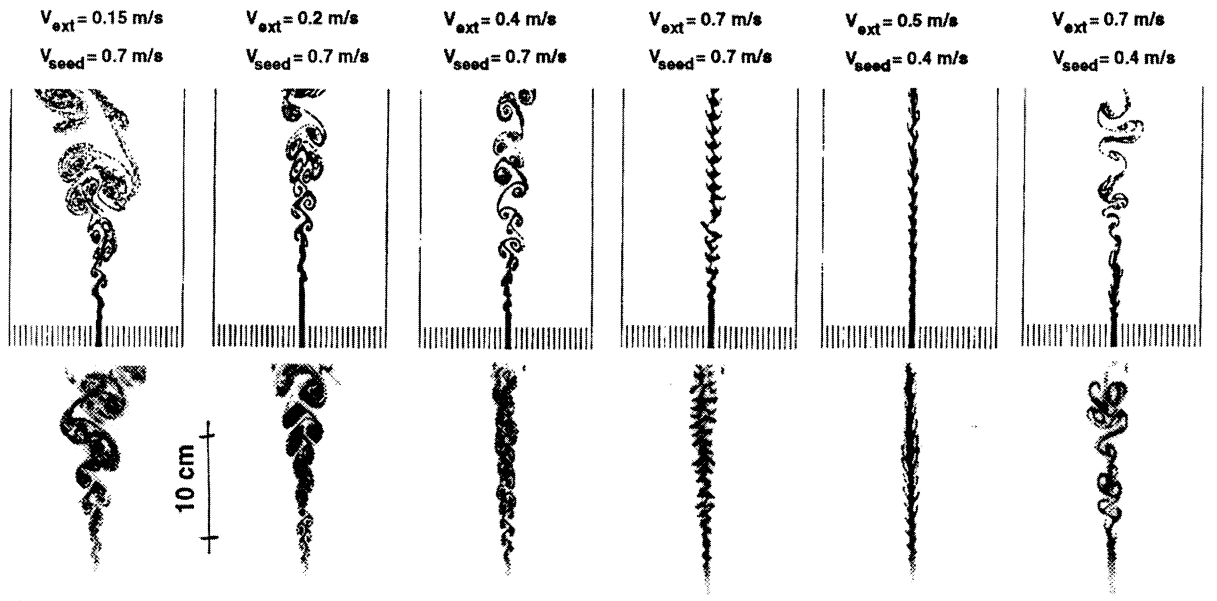

Fig. 18. Examples of interfaces of 2D transitional flows. In the upper row are reported the numerical prediction (after Cavaliere et al. [173,174]) while in the lower row the laser light scattering images are reported (due to the presence of sub-micronic seeding in the flow) in the corresponding conditions.

quantities, as temperature and concentration, or of fluid-dynamic structures, affecting these quantities in turbulent diffusion flames may be obtained in 2D time-dependent flows. This is due to the basic principle that chaotic flows can be created also in laminar deterministic periodic conditions [12,20]. The only additional requirement is that stagnation points have to be distributed in such a way, respect to a reference frame moving with the average velocity, that the stretch ratio of material lines undergo exponential evolution. The high level of stretching is the main feature of dissipative highly diffusive turbulent flow, i.e. the most important factor for increasing mixing rate, consequently combustion rates, and extinguish-related effects.

The other requirements, which 2D time-dependent flows have to fulfill in order to be representative of 3D turbulent flow, is the high level of convolution of interfaces, and their distribution on different length scales. The only concern is related to the capability of 2D flows of being exhaustive in containing all possible fluid-dynamic structures, which are present in 3D turbulent flows.

In order to give an assessment of the great variety of structures which can be established in 2D flows, interfaces, obtained in 2D, are reported in Fig. 18.

They are relative to gaseous flows introduced into a main channel (18 cm width) through 32 equal channels. The layout of this confinement can be seen in the upper row. The average velocity of central channel is 0.7 m s^{-1} in the first four cases and 0.4 m s^{-1} in the last two cases.

The external velocity is varied between 0.15 and 0.7 m s^{-1}. The upper row is relative to numerical predictions in which the streak-lines of material points, 'injected' at the inflow boundary, have been computed. The lower row is relative to pattern of laser light scattered by a sub-micron seeding. Computational and experimental details and the choice of the boundary conditions are not relevant here and they are reported in the references [173,174]. It is of great interest to underline that the comparison is quite satisfactory and that, in turn, this shows the two-dimensionality of the flows. Among these flows, there are some of them, pertaining to highest ratio between the external and central velocity, in which the interfaces (discontinuity between black and white regions) are quite convoluted, as it is possible to observe in the figure. They undergo a relatively intense stretch rate of the order of 100 s^{-1}, as it has been reported elsewhere [24]. This stretch rate is not high enough to cause flame extinction, but it is sufficient for high level of convolution.

The examples, here described, suggest that ensemble of structures, i.e. a simple multi-scale system, can be used in order to explore all possible evolution of the system itself. Section 2.2.3, together with the following one, shows how this tool can be exploited to identify mixing isothermal regimes and to give statistical averages of the most relevant parameter affecting the diffusion flames. Another wide field of its application is only briefly quoted here even though it has great momentum from technological and basic point of view, i.e. transitional flows. The mechanistic aspects of the transition have been reviewed in isothermal [175] and reactive flow [176]. The identification of the first modes excited by internal and external fluid-dynamic effects [177–179]

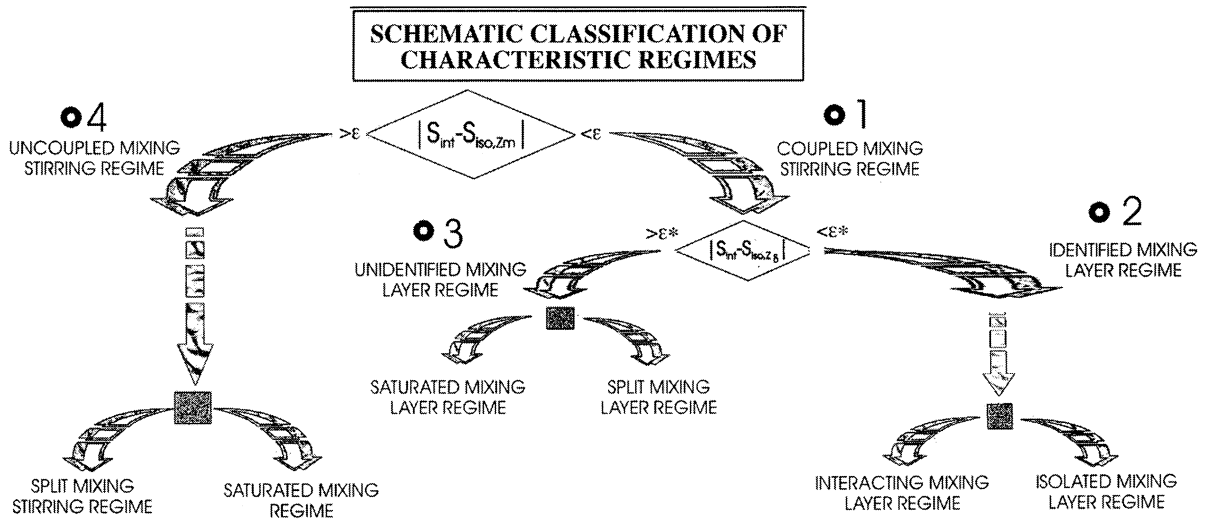

Fig. 19. Schematic classification of characteristic regimes.

has been focused as first target. Then other features have been studied in 2D field, like flame stability at transitional point [180]. These results are extension of validity of those obtained in turbulent regimes [181,182] also in respect of different boundary conditions [183]. These types of flows have been exploited also for detecting single diffusive structures, in reacting or isothermal conditions. This use has been implicitly quoted in the description of 2D vortical structures.

Finally some peculiar diagnostics applications have been made possible only because they have been used in 2D flow systems. This is the case of Lagrangian measurements, as it has been discussed in Section 2.

5.2.2. Classification of mixing regimes

A classification of mixing regimes can be done with the help of Fig. 19. It can be seen as a physical and logical flow chart based on the analysis of the plot on the right side of Fig. 3.

The first test, in the figure above, considers the comparison of the progressive interface (line 1 of Fig. 3) and progressive isosurfaces selected at the overall mixture fraction Z_m (line 5 of Fig. 3). The two surfaces are coincident before a 'splitting time', which is shown as t_{s_2} in the example of Fig. 3. In this case the evolution of the molecular mixing can be analyzed in relation to the interface. In fact the stretching and the folding involve both surface. The regime is defined as a 'coupled mixing–stirring regime' (route 1 in the figure) when the flow satisfies the above conditions. On the other hand, when the difference between the area of the progressive interface and of the progressive isosurface is greater than a fixed conventional value the flow is classified as an 'uncoupled mixing stirring regime' (route 4 in the figure). A further division can be obtained in the 'coupled mixing stirring regime' category using a criteria based on the aforementioned area difference in which the progressive isosurface is relative to the typical value of the periphery of the mixing layer. The value of the mixture fraction at $Z = 0.05$ and $Z = 0.95$, used in the example of Fig. 3 can be considered a reasonable approximations of these peripheral values. When the area difference is smaller than a prefixed arbitrary value for both progressive isosurfaces the entire mixing layer develops in the vicinity of the interface and has a recognisable pattern. Thus, the flows, or parts of the flows that satisfy these properties, can be considered as belonging to an 'identified mixing layer regime' (route 2 in the figure). The other possible case can be classified as 'unidentified mixing layer regime' (route 3 in the figure). The mixing layer can disappear either due to annihilation of the surfaces of constant property (which always entails a decrease of isosurface extension or equivalently, a non-increase of the progressive isosurface) or due to a positive stretching along the direction of the mixture fraction gradient. In the latter case, surfaces at constant Z separate from each other following different kinetic evolution. The flows, which are in these conditions, are labelled in the figure as 'split mixing layer' regimes. The same type of comment can highlight significant differences between the progressive isosurface relative to the overall mixture fraction value Z_m. In this case the flows are classified, as mentioned before, 'uncoupled mixing stirring' regimes thus the two processes are totally uncorrelated and the interface is no longer a point of reference for the analysis of constant property surfaces. Here too this regime can be sub-divided into two further classes with reference to the annihilation or separation of the isosurfaces. The first class is named 'saturated mixing regime' in analogy with the previous one, the second 'split mixing stirring' regime.

It is worth stressing that a 2D simulation of a prototypal flow pattern has been used for the analysis. As a consequence, the extension of the classification criteria to 3D

cases and the experimental validation are both needed for a more general confidence in the classification. In any case it should be clear that the classification keeps an intrinsic validity which is not based on the flow simulation. In fact this was exploited in order to exemplify possible evaluations on specific mixing processes.

Finally it is useful to classify the regimes following the route 2, in which the mixing layer is identifiable, into two classes. These are named 'interacting' or 'isolated' mixing regimes, according to the distance and the level of interaction between different parts of the mixing layers.

The progressive interface and isosurface are quantities that have been defined here for the first time, so that the previous experience in their measurement cannot be found in literature. However, it is clear that the difficulty in their measurement lies in their Lagrangian aspect. In fact, feasibility of detection of a progressive isosurface relies on the possibility of injecting either a non-diffusive or diffusive tracer starting from the arbitrary time t_0. This is a difficult task if the transition, from absence to presence of tracer, has to be ensured at the same time on the whole inflow boundary. In fact the tracer injection on the inlet boundary can interfere with fluid-dynamic inflow conditions and it cannot be anticipated upstream of the boundary without pre-stirring or pre-mixing the traced and non-traced flows. Techniques based on smoke wire devices or on photocromic tracers, which change their physical/optical properties crossing light sheet on the boundary, are possible candidates to generate identifiable progressive interface and isosurface.

5.2.3. Evolution and statistics of 3D fields in 2D representations

Turbulent flows are characterized by a high level of three-dimensionality. This entails the aforementioned (Sections 3.1 and 3.3) difficulties in numerical and experimental analysis particularly linked to simultaneous characterizations of a wide scale range when the dimensionality is increased. Nevertheless a rich source of information on mechanistic and statistical evolutions comes from two different approaches. The first consists in the 2D pattern measurements of scalar quantities with such precision that gradient and scalar dissipation rates can be evaluated too [42,150,183–185]. The merits and the limits of these schemes as well as specific information on the procedures and on the results are well described in the quoted papers. As example of the potential of this approach, a sketch (Fig. 20a) of the flammable mixture boundary of propane–air turbulent jet is reproduced in the above frame as the authors of an aforementioned paper [184] have really measured. They have also measured the scalar dissipation rate χ, which is outlined in the sketch with shaded area representative of regions where χ is higher than a fixed value. χ can also be obtained as conditional statistics inside the flammable mixture. The outstanding feature is that the mixture fraction distribution in the example is such that it shows the distribution of positive and negative stretch along the stoichiometric surfaces similar to that predicted by Ashurst and Williams [150]. The second approach consists in Direct Numerical Simulation (DNS) [37] of '2D turbulent' reactive flows. This has been much used in the past few years in order to obtain indications about group behavior of several quantities, that have been proved to be of interest in the evolution of simple structures and that have been hypothesized to be controlling in 3D turbulent diffusion flames too. For example in Fig. 20b, the scheme of a fluid-dynamic condition is shown, used by Van Kalmthout et al. [38] according to the profile reported in the lower part of the same figure. In order to conduct this type of study they injected gaseous flows with a 0 mixture fraction, on the left-hand side (the oxidant), and 1, on the right side (fuel). The two flows are kept in a turbulent regime by the addition of isotropic homogenous turbulent fluctuations with a predetermined 'von Kármán–Pao' power spectrum. The evolution of the resulting flow is followed as already mentioned, by means of a direct 2D simulation. In the frame, the 2D pattern on the left-hand side represents three isosurfaces at $Z = 0.25$, 0.50 and 0.75 by means of a thick line and various surfaces of isovorticity by thin lines. The plot on the right hand side (Fig. 20c) shows the fluid-dynamic stretch rate $K^{\mathrm{v}}_{\delta A_Z}$, averaged along stoichiometric surfaces, versus the mixture fraction Z. The thick continuous line follows the values obtained from the numerical experiment, while the thin continuous line is a modeled constant value. The stretch rate caused by the curvature, $K^{\mathrm{w}}_{\delta A_Z}$, reported with a thick dotted line, is obtained as the sum of two terms, according to Eq. (5), as detailed here below

$$K^{w}_{\delta A_Z} = \langle w \boldsymbol{\nabla}\cdot n\rangle_{\delta A_Z} = A + B \tag{32}$$

$$A = -\mathscr{D}_Z \langle (\boldsymbol{\nabla}\cdot\mathbf{n})^2\rangle_{\delta A_Z} \tag{33}$$

$$B = -\left\langle \frac{\mathscr{D}_Z}{|\nabla Z|}\frac{\partial|\boldsymbol{\nabla} Z|}{\partial x_{\mathrm{n}}}\boldsymbol{\nabla}\cdot\mathbf{n}\right\rangle_{\delta A_Z} \tag{34}$$

The two terms are represented by means of the segmented lines with short dashes (A) and with long dashes (B), respectively.

It is immediately noticeable that the term caused by fluid-dynamic prevails over that relative to the propagation of the curved isosurface, and that in the case in hand (absence of mean velocity gradients) both stretch rates are approximately constant. The authors show that this kind of behavior is true also for other values in the stoichiometric ratios.

Solutions of compressible full Navier–Stokes equations, associated with equations pertaining reaction conditions have also been presented [64,186] for the study of mixing layers at high Re. The interested reader is addressed to the last two articles for a deeper understanding.

5.3. Simple 3D systems

There are not many detailed descriptions of ensembles of

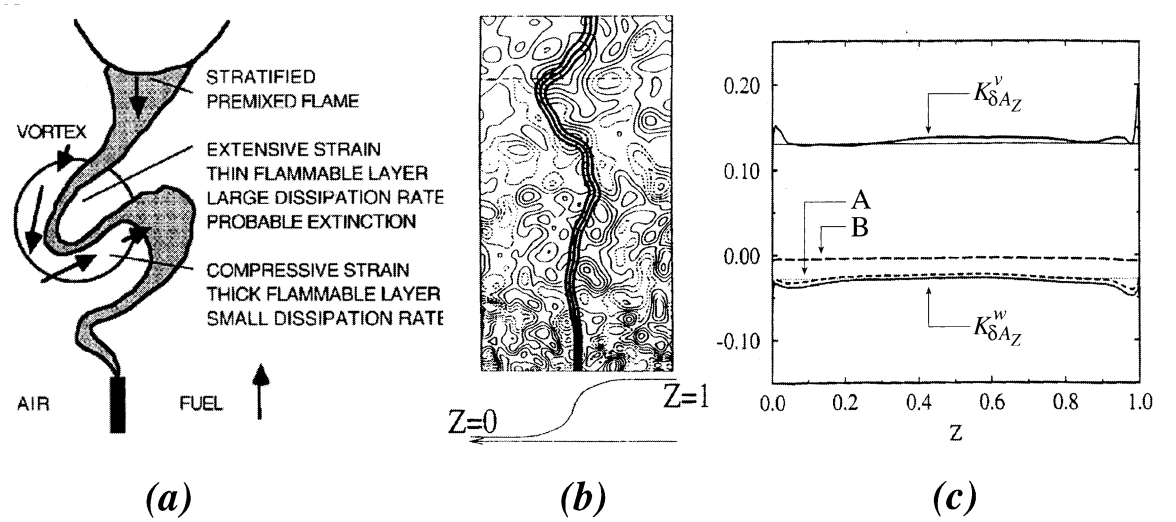

Fig. 20. (a) Example of flammable mixture boundary (after Everest et al. [184]). (b) Examples of isosurfaces at constant mixture fraction (at $Z = 0.25$, 0.5, 0.75, thick lines) and vorticity (thin lines), after Van Kalmthout et al. [38]. (c) Contributions to stretch rates on isosurface at mixture fraction reported on the abscissa. Adapted from Van Kalmthout et al. [38].

structures in 3D fields. This is due to the difficulty mentioned in the previous section. Therefore the studies which are quoted here refer to complete 3D simulations of flow in control volume, whose dimension is only few orders of magnitude higher than the smallest resolvable length-scales. Low Reynolds number or transitional flows belong to this category. They may develop ensembles of structures in a narrow range of length scales so that they are suitable for some experimental validation too. Relatively high Reynolds number turbulent flows, in which only the small length-scales are simulated, are also of interest. In this case initial turbulent kinetic energy spectra and periodic boundary conditions are generally prescribed and mixing–reacting fields are simulated in decaying turbulent fields.

The first category of flows has been explored in order to characterize laminar or transitional flows, which are 3D from the beginning near the inlet in the case of a non-circular jet. An example of the potentials in outlining topological features of interest in the diffusion flame characterization is given in the left side of Fig. 21 reproduced from a recent paper [187]. Patterns of scalar dissipation rates χ on vertical and horizontal cross-sections are also shown. The authors stress the sheet like structures of the distribution of χ.

The second category of papers has been mainly devoted to the assessment of turbulence kinetics mechanisms [188]. The plot on the right side of Fig. 21 shows an example of results obtained in this work. The stretch rates integrated on the whole isosurface (ΔA_Z), contained in the control volume, at different mixture fraction, Z

$$I = \oiint_{\Delta A_Z} K^{\mathrm{v}}_{\delta A}\, \mathrm{d}A \tag{35}$$

vs Z itself are shown. The dotted line indicates that the whole fluid-dynamic stretch rate is taken into account, according to Eq. (7). A dashed/dotted line corresponds to the incompressible part (I^{i})

$$K^{\mathrm{v}}_{\delta A}|_i = \mathbf{nn} : \boldsymbol{\nabla}\mathbf{v} \tag{36}$$

Same values of these two integrals occur in the mixture fraction range between 0.5 and 0.6, which are representative of the stoichiometric values used in this work ($Z = 0, 5$). Approximately equal values are also present for the unmixed conditions $Z = 0$ and $Z = 1$. Only integrals relative to intermediate mixture fractions around $Z = 0.15$ and $Z = 0.85$ are quite different. It is of interest to note that expansion rate, due to heat release around stoichiometric value, is not responsible of the corresponding isosurface stretch. In fact the difference between the corresponding values on the two curves represents the compressible contribution and it is quite negligible at $Z = 0.5$. The third profile drawn with solid line (I^{w}) is the integral of the stretch rate due to the diffusive propagation of a curved isosurface, as it has been expressed in the equation of the previous section, $K^{\mathrm{w}}_{\delta A_Z}$. The contribution to the total stretch of this part is quite smaller than that shown in the 2D 'turbulent' field. In this case it is nearly negligible but positive in a wide range of the mixture fraction. Only the unmixed fuel region presents a significant negative stretch. The greater relevance of the fluid-dynamic stretch has been also shown in 2D turbulent fields [37] quoted in the previous section. A study more related to chemical kinetic rates has been devoted to the mechanistic analysis of presence of species in super-equilibrium concentration in reactive 3D flow [189]. Also in this case the kinetic model, used in the work, was a two-step reactions one, in which an intermediate species was

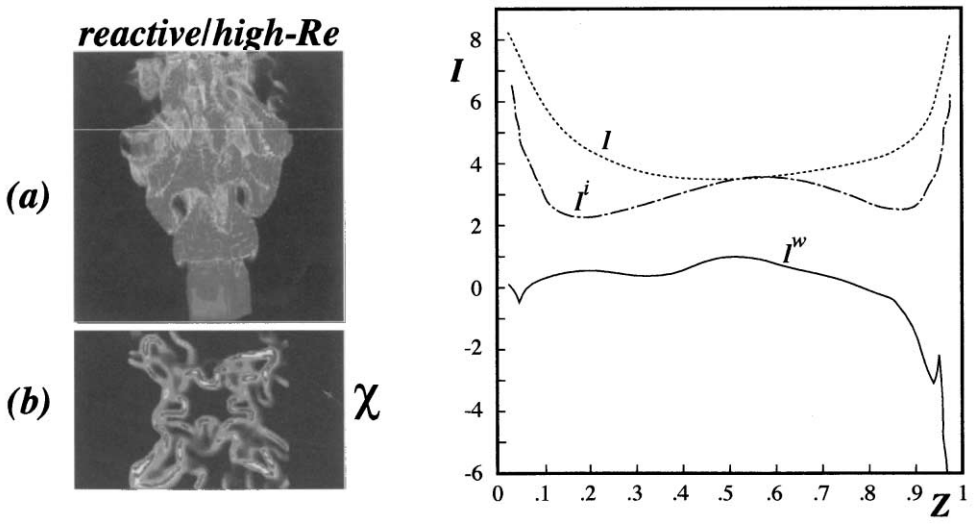

Fig. 21. On the left side: example of scalar dissipation rates on vertical (a) and horizontal (b) cross-section (after Grinstein and Kailasanath [187]). On the right side: example of stretch rates integrated (I) on an isosurface at mixture fraction Z, reported on the abscissa. I^i and I^w curves are the contribution to I due to incompressible evolution and diffusive propagation.

considered representative of radical or other partial oxidation product. The main result was the confirmation that local stretching is responsible of partial quenching of diffusive reactive structures. This role, i.e. validation of results obtained in lower dimensional fields, seems to be the most suitable one for the studies exploiting 3D DNS. This attains to identification either of single structure or of significant statistical averages in transitional as well as turbulent regimes.

6. Conclusion

This paper has reviewed works dealing with single diffusive structures, with their mutual interaction in simple flows and their relevance in statistical modeling in complex flows. The focus has been given to conditions pertaining to gaseous diffusion flames, but also isothermal structures have been described when they were related to combustion regimes.

It is worthwhile to stress that this review was not devoted to the topic of reacting flows in turbulent regimes. Therefore it could seem to be overabundant to have presented even few topics dealt in this field or inappropriate to have a bias toward the only selected ones. As matter of fact, this is not the case since the very few turbulent subjects, presented in the paper have been chosen with a well-defined purpose. It consists in showing a perspective view of the possible exploitation of the knowledge about simple structures in numerical modeling of complex flows. In this respect the choice of the topics reported for instance in Sections 2.2.3 and 2.2.4 is subjective, in the sense that it has not yet proved its full capability in the satisfactory modeling of turbulent diffusion flames. Nevertheless it uses the same quantities, which are involved in the description of simple structures, and the statistical averaging of these quantities may be easily interpreted in terms of processes and phenomena discussed in the paper.

It is of interest to note that experimental analyses of turbulent diffusion flames are based on the characterization of multi-component reacting flows by means of data acquired from single point measurements and are usually organized as scalar scatter-plots. A very exhaustive review of this approach has been quoted before [43]. At the same time the reader should be aware that this approach is zero-dimensional, in the sense that it is based on single point Eulerian measurements, whereas the exploitation of diffusive structures is mainly based on evaluation of multi-dimensional and Lagrangian quantities. It has been discussed in Section 3.1 that first approach is feasibly pursuable in the experimental statistical characterization of many complex flows, whereas it has been shown along the whole review that the second one is effective only in the analysis of relatively simple flows. Therefore the complementary nature of the two approaches and the role of the second one in the understanding and modeling of the physical and chemical processes only from a conceptual point of view should also be deeply considered.

Finally it is noteworthy to comment that the review shows how rich and variegate the literature dealing with unidimensional structures is. It seems that all possible effects related to them have been captured. Only studies pertaining to new fuels or new peculiar boundary conditions are expected to exploit such simplified configurations in order to enlarge the basic knowledge with respect to specific conditions.

2D structures are the object of the most active and recent research work. In particular, they contribute to understand

the effect of curvature and annihilation on complex structures as it has been documented in this paper as well as to enhance mixing, shaping and stabilization control in diffusion flame stabilization [146].

3D diffusion flames structures have been rarely analyzed and exploited in well defined frameworks therefore the potentials which they can offer to understand turbulent diffusion flames, particularly in relation to different length scales interactions, is not clear at the moment. In this respect this topic represents one of the most advanced research forefronts, which deserves a coordinated effort in order to assess the exhaustiveness of uni/bidimensional structures in describing turbulent flames and possibly to identify new regimes as well as new kinds of effects in stirring/mixing/reacting fields.

Appendix A

The 'mixing fraction', $Z \circ \xi$, is defined as

$$Z = \xi = \frac{\beta - \beta_2}{\beta_1 - \beta_2} \tag{A1}$$

where β is a conservative variable and the subscripts 1 and 2 refer to fuel and oxidant streams, respectively. $Z(\xi)$ is a non-dimensional number ranging between 0 and 1.

Examples of conservative variables are mass fraction and enthalpy. The mass fraction of fuel and oxidant are defined as

$$Y_{(C,H)} = \sum a_{Ci} \frac{m_C}{m_i} Y_i + \sum a_{H,i} \frac{m_H}{m_i} Y_i \tag{A2}$$

$$Y_{(O)} = \sum a_{O,i} \frac{m_o}{m_i} Y_i \tag{A3}$$

Subscripts C, H, and O in parentheses refer to carbon, hydrogen and atomic oxygen that are either bonded or not bonded to any chemical species in a predefined control mass.

As a consequence $Y_{(C,H)}$ is the mass fraction of the total carbon and atomic hydrogen contained in all the chemical species present in a control volume whose density is ρ. a_{Cj}, a_{Hj}, a_{Oj} are the numbers of C, H and O atoms in the ith species. $Y_{(C,H)}$ represents the fuel mass fraction that has either reacted or not. In other words $Y_{(C,H)}$ could be also indicated as Y_{comb}.

The mixing fractions $Y_{(C,H)}$ and $Y_{(O)}$ can be written as

$$Z_f = \xi_f = \frac{Y_{(C,H)} - Y_{(C,H)2}}{Y_{(C,H)1} - Y_{(C,H)2}} = \frac{Y_{(C,H)}}{Y_{(C,H)1}} \tag{A4}$$

$$Z_o = \xi_o = \frac{Y_{(O)} - Y_{(O)2}}{Y_{(O)1} - Y_{(O)2}} = 1 - \frac{Y_{(O)}}{Y_{(O)2}} \tag{A5}$$

The last members of Eqs. (4) and (5) are true when there is no fuel in the oxidizing flow ($Y_{(C,H)_2} = 0$) and there is no oxidizer in the fuel flow ($Y_{(O)_1} = 0$). Z_f and Z_o are equal when equidiffusion can be assumed.

This statement will be proved in the hypothesis that diluting species in the oxidant and fuel flow are also present. In this case in the flow 1 will be present, in addition to the fuel mass fraction $Y_{(C,H)_1}$, a diluent whose mass fraction is

$$1 - Y_{(C,H)_1} = Y_{(C,H)_1} \frac{1 - Y_{(C,H)_1}}{Y_{(C,H)_1}} \tag{A6}$$

In other words the diluent in the flow 1 has a mass fraction $\eta = (1 - Y_{(C,H)_1})/Y_{(C,H)_1}$ of the fuel mass fraction. Analogously, under the same equidiffusion hypothesis, in any point of the flow a diluent mass fraction

$$Y_{(C,H)} \eta \tag{A7}$$

will be associated to the fuel mass fraction $Y_{(C,H)}$.

The same discussion could be applied to the oxidant mass fraction $Y_{(O)}$ to which will be associated a diluent mass fraction

$$Y_{(O)} \frac{1 - Y_{(O)_2}}{Y_{(O)_2}} \tag{A8}$$

By imposing that the sum of all the mass fractions is unity it results that

$$Y_{(C,H)_1} + Y_{(C,H)_1} \frac{1 - Y_{(C,H)_1}}{Y_{(C,H)_1}} + Y_{(O)} + Y_{(O)} \frac{1 - Y_{(O)_2}}{Y_{(O)_2}} = 1 \tag{A9}$$

and by evidencing $Y_{(C,H)}$ and $Y_{(O)}$

$$Y_{(C,H)_1} \left(1 + \frac{1 - Y_{(C,H)_1}}{Y_{(C,H)_1}}\right) + Y_{(O)} \left(1 + \frac{1 - Y_{(O)_2}}{Y_{(O)_2}}\right) = 1 \tag{A10}$$

and

$$Y_{(C,H)} \left(\gamma + \frac{1}{Y_{(C,H)_1}} - \gamma\right) + Y_{(O)} \left(\gamma + \frac{1}{Y_{(O)_2}} - \gamma\right) = 1 \tag{A11}$$

that is

$$\frac{Y_{(C,H)}}{Y_{(C,H)_1}} = 1 - \frac{Y_{(O)}}{Y_{(O)_2}} \tag{A12}$$

or

$$Z_f = Z_o \tag{A13}$$

Another important relation is regarding the mixing fraction in correspondence of the stoichiometric ratio ν_s. The mixing fractions will be indicated with the subscript s when

$$\nu_s = Y_{(O)}/Y_{(C,H)} \tag{A14}$$

that can be expressed as

$$Z_{st} = \xi_{st} = \left(1 + \nu_s \frac{Y_{(C,H)_1}}{Y_{(O)_2}}\right)^{-1} \tag{A15}$$

This expression comes from

$$Z_{st} = 1 - \frac{Y_{(O)_{st}}}{Y_{(O)_2}} \rightarrow Z_{st} = 1 - \frac{\nu_s \, Y_{(C,H)_{st}}}{Y_{(O)_2}} \tag{A16}$$

$$Z_{st} = \frac{Y_{(C,H)_{st}}}{Y_{(C,H)_1}} \rightarrow Y_{(C,H)_{st}} = Z_{st} Y_{(C,H)_1} \tag{A17}$$

and substituting Eq. (17) in Eq. (16) results in

$$Z_{st} = 1 - \frac{\nu_s Z_{st} Y_{(C,H)_1}}{Y_{(O)_2}} \tag{A18}$$

That allows us to obtain Z_{st} as

$$Z_{st} Y_{(O)_2} - Y_{(O)_2} + \nu_s Z_{st} Y_{(C,H)_1} = 0 \tag{A19}$$

$$Z_{st}(Y_{(O)_2} + \nu_s Y_{(C,H)_1}) = Y_{(O)_2} \tag{A20}$$

$$Z_{st}\left(1 + \nu_s \frac{Y_{(C,H)_1}}{Y_{(O)_2}}\right) = 1 \tag{A21}$$

and also

$$Z_{st} = \xi_{st} = \left(1 + \nu_s \frac{Y_{(C,H)_1}}{Y_{(O)_2}}\right)^{-1} \tag{A22}$$

Appendix B

The following derivation of the strain rate K over a surface δA has been reported from Candel and Poinsot [190] and comes from the formulation of the transport theorem given by Aris [191]

$$\frac{\mathrm{d}}{\mathrm{d}t}\int\int_S \mathbf{a}\cdot\mathbf{n}\,\mathrm{d}S = \int\int_S \left[\frac{\partial \mathbf{a}}{\partial t} + (\boldsymbol{\nabla}\cdot\mathbf{a})\mathbf{v} + \boldsymbol{\nabla}\wedge(\mathbf{a}\wedge\mathbf{v})\right]\cdot\mathbf{n}\,\mathrm{d}S \tag{B1}$$

taking in account that

$$\boldsymbol{\nabla}\wedge(\mathbf{a}\wedge\mathbf{v}) = \mathbf{v}\cdot\boldsymbol{\nabla}\mathbf{a} - \mathbf{a}\cdot\boldsymbol{\nabla}\mathbf{v} - \mathbf{v}\boldsymbol{\nabla}\cdot\mathbf{a} + \mathbf{v}\boldsymbol{\nabla}\cdot\mathbf{a} \tag{B2}$$

it follows:

$$\frac{\mathrm{d}}{\mathrm{d}t}\int\int_S \mathbf{a}\cdot\mathbf{n}\,\mathrm{d}S = \int\int_S \left[\frac{\partial \mathbf{a}}{\partial t} + \mathbf{v}\cdot\boldsymbol{\nabla}\mathbf{a} + \mathbf{a}(\boldsymbol{\nabla}\cdot\mathbf{v}) - (\boldsymbol{\nabla}\cdot\mathbf{a})\mathbf{v}\right]\cdot\mathbf{n}\,\mathrm{d}S \tag{B3}$$

Eq. (B3) can be applied to any vectorial quantity defined over a surface $S(t) = \delta A(t)$. Assuming a equal to the unitary vector normal to the surface $\mathbf{n}$ it follows:

$$\frac{\mathrm{d}}{\mathrm{d}t}\int\int_{\delta A(t)} \mathrm{d}\delta A = \int\int_{\delta A(t)} \left[\frac{\partial \mathbf{n}}{\partial t} + \mathbf{v}\cdot\boldsymbol{\nabla}\mathbf{n} + \mathbf{n}(\boldsymbol{\nabla}\cdot\mathbf{v}) - (\boldsymbol{\nabla}\cdot\mathbf{n})\mathbf{v}\right]\cdot\mathbf{n}\,\mathrm{d}\delta A \tag{B4}$$

and since

$$\frac{\partial \mathbf{n}}{\partial t}\cdot\mathbf{n} = \frac{1}{2}\frac{\partial}{\partial t}n^2 = 0 \tag{B5}$$

$$(\mathbf{v}\cdot\boldsymbol{\nabla}\mathbf{n})\cdot\mathbf{n} = \mathbf{v}\cdot\boldsymbol{\nabla}\left(\frac{1}{2}n^2\right) = 0 \tag{B6}$$

it follows:

$$\frac{\mathrm{d}}{\mathrm{d}t}\int\int_{\delta A(t)} \mathrm{d}\delta A = \int\int_{\delta A(t)} [-\mathbf{nn} : (\boldsymbol{\nabla}\mathbf{v}) + \cdot\mathbf{v}]\,\mathrm{d}\delta A \tag{B7}$$

and, considering that the integrand in the second term is constant, it follows:

$$\frac{1}{\delta A}\frac{\mathrm{d}\delta A}{\mathrm{d}t} = -\mathbf{nn} : (\boldsymbol{\nabla}\mathbf{v}) + \boldsymbol{\nabla}\cdot\mathbf{v} \tag{B8}$$

Analogously it could be demonstrated that, as it has been reported by Ottino (37), that a linear element δl and a volume element δV are stretched according to the laws

$$\frac{1}{\delta l}\frac{\mathrm{D}\delta l}{\mathrm{D}t} = (\boldsymbol{\nabla}\mathbf{v}) : \mathbf{mm}$$

$$\frac{1}{\delta V}\frac{\mathrm{D}\delta V}{\mathrm{D}t} = (\boldsymbol{\nabla}\mathbf{v}) : \mathbf{uu} = \boldsymbol{\nabla}\cdot\mathbf{v}$$

where $\mathbf{m}$ and $\mathbf{u}$ are the tangential versor to the linear element and the unitary versor, respectively.

By substituting $\mathbf{v} = \mathbf{v}_t + \mathbf{n}v_n$ in Eq. (B8) it follows:

$$\boldsymbol{\nabla}(\mathbf{v}_t + \mathbf{n}v_n) - \mathbf{nn} : \boldsymbol{\nabla}(\mathbf{v}_t + \mathbf{n}v_n)$$

$$= \boldsymbol{\nabla}\cdot\mathbf{v}_t + \boldsymbol{\nabla}\cdot\mathbf{n}v_n - \mathbf{nn} : \boldsymbol{\nabla}\mathbf{v}_t - \mathbf{nn} : \boldsymbol{\nabla}\mathbf{n}v_n \tag{B9}$$

and since $\mathbf{nn} : \boldsymbol{\nabla}\mathbf{v}_t = 0$

$$\boldsymbol{\nabla}(\mathbf{v}_t + \mathbf{n}v_n) - \mathbf{nn} : \boldsymbol{\nabla}(\mathbf{v}_t + \mathbf{n}v_n)$$

$$= \boldsymbol{\nabla}\cdot\mathbf{v}_t + \mathbf{n}\cdot\boldsymbol{\nabla}v_n + v_n\boldsymbol{\nabla}\cdot\mathbf{n} - \mathbf{nn} : \boldsymbol{\nabla}(\mathbf{n}v_n) \tag{B10}$$

And since $\mathbf{n}\cdot\boldsymbol{\nabla}v_n$ is equal to $\mathbf{nn} : \boldsymbol{\nabla}(\mathbf{n}v_n)$ it results

$$\boldsymbol{\nabla}\cdot\mathbf{v} - \mathbf{nn} : (\boldsymbol{\nabla}\mathbf{v}) = \boldsymbol{\nabla}\cdot\mathbf{v}_t + v_n\boldsymbol{\nabla}\cdot\mathbf{n} \tag{B11}$$

Appendix C

We want now to determine the concentration profile or the mixture fraction in the unsteady 1D case

$$\frac{\partial Z}{\partial t} = D\frac{\partial^2 Z}{\partial x^2} \tag{C1}$$

for this it was helpful to use the Boltzmann variable

$$\xi = \frac{x}{\sqrt{Dt}} \tag{C2}$$

by substituting in Eq. (C1)

$$\frac{\mathrm{d}Z}{\mathrm{d}\xi}\left(\frac{\partial \xi}{\partial t}\right) = D\frac{\mathrm{d}^2 Z}{\mathrm{d}\xi^2}\left(\frac{\partial \xi}{\partial x}\right)^2 \tag{C3}$$

and since

$$\frac{\partial \xi}{\partial t} = \frac{x}{\sqrt{4D}}(-1/2t^{3/2}) = \frac{-x}{2t\sqrt{4Dt}} \tag{C4}$$

$$\frac{\partial \xi}{\partial x} = \frac{1}{\sqrt{4Dt}}$$

Eq. (C1) becomes

$$\frac{d^2Z}{d\xi^2} + 2\xi\frac{dZ}{d\xi} = 0 \tag{C5}$$

with the boundary conditions

$$x = 0 \Rightarrow \xi = 0 \qquad Z = Z_0 \tag{C6}$$

$$x \to \infty \Rightarrow \xi = \infty \qquad Z = Z_\infty$$

By introducing the quantity

$$y = \frac{\partial Z}{\partial \xi} \tag{C7}$$

Eq. (C5) can be easily resolved as

$$\frac{\partial y}{\partial \xi} + 2\xi y = 0$$

$$\frac{dy}{y} = -2\xi\, d\xi$$

$$\ln y = -\xi^2$$

and in terms of Z

$$y = a\, e^{-\xi^2} \Rightarrow \frac{\partial Z}{\partial \xi} = a\, e^{-\xi^2} \tag{C8}$$

$$[Z]_o^\xi = a\int_o^\xi e^{-\xi^2}$$

$$Z - Z_o = a\int_o^\xi e^{-\xi^2}$$

By evaluating at $\xi \to \infty$ it is possible to determine the value of the constant a

$$Z - Z_0 = a\cdot\int_0^\infty e^{-\xi^2}\, d\xi = a\frac{\sqrt{\pi}}{2} \tag{C9}$$

$$a = 2\cdot\frac{(Z - Z_0)}{\sqrt{\pi}}$$

and by substituting

$$\frac{Z(x,t) - Z_o(x=0,t)}{Z_\infty(x=\infty,t) - Z_o(x=0,t)} = \frac{2}{\sqrt{\pi}}\int_o^\xi e^{-\xi^2} = \mathrm{erf}(\xi) \tag{C10}$$

finally

$$\frac{Z - Z_0}{Z_\infty - Z_0} = \mathrm{erf}(\xi) \tag{C11}$$

where

$$\xi = \frac{x}{\sqrt{4Dt}}.$$

If the boundary conditions are given at $-\infty$ and $+\infty$

$$\begin{aligned} &x = -\infty \quad \xi = -\infty \quad Z = 0 \\ &x = \infty \qquad \xi = \infty \qquad Z = Z_\infty \end{aligned} \tag{C12}$$

Eq. (C8) is

$$[Z]_{-\infty}^\xi = a\int_{-\infty}^\xi e^{-\xi^2}\, d\xi \tag{C13}$$

and performing the same calculations

$$Z(x=\infty) - Z(x=-\infty) = a\int_{-\infty}^{+\infty} e^{-\xi^2} = 2a\int_o^{+\infty} e^{-\xi^2} = a2\cdot\frac{\sqrt{\pi}}{2} \tag{C14}$$

$$a = \frac{Z_\infty}{\sqrt{\pi}} \Rightarrow Z(x,t) = \frac{Z_\infty}{\sqrt{\pi}}\int_{-\infty}^{+\infty} e^{\frac{-x^2}{4Dt}}\, dx$$

and finally

$$\frac{Z}{Z_\infty} = \frac{1}{2}\mathrm{erf}(\xi) \tag{C15}$$

Appendix D

We want now to find the expression for Z in the case of an unsteady convective mixing layer under the hypothesis of linearizable velocity.

In this case it is possible to approximate the equation

$$\frac{\partial Z}{\partial t} + u\frac{\partial u}{\partial x_n} - D\frac{\partial^2 Z}{\partial x_n^2} = 0$$

as

$$\frac{\partial Z}{\partial t} - Kx_n\frac{\partial Z}{\partial x_n} - D\frac{\partial^2 Z}{\partial x_n^2} = 0 \tag{D1}$$

where

$$K = -\frac{\partial u_n}{\partial x_n} = \frac{1}{\delta A}\frac{D(\delta A)}{Dt} \tag{D2}$$

is the 'stretch rate' and is related to the stretch ratio

$$\mathrm{SR} = \frac{(\delta A)_t}{(\delta A)_{t_o}} \tag{D3}$$

by the equation

$$\int_{t_o}^t K\, dt = \int_{t_o}^t \frac{D(\delta A)}{\delta A} = \ln\left[\frac{(\delta A)_t}{(\delta A)_{t_o}}\right] = \ln \mathrm{SR} \tag{D4}$$

that is

$$\mathrm{SR} = \exp\left[\int_{t_o}^t K\, dt\right] \tag{D5}$$

Following the suggestion of Chella and Ottino (10) we can make the substitution

$$\xi(x_n, t) = x_n f(t) \tag{D6}$$

$$\tau = \tau(t) \tag{D7}$$

and (as a consequence of Eq. (D6))

$$\left\{\frac{\partial \xi}{\partial x_n} = f(t),\ \frac{\partial \xi}{\partial t} = x_n f(t)\right\}$$

Assuming that Z depends on the two variables ξ and τ

$$Z = Z(\xi, \tau) \tag{D8}$$

and substituting in Eq. (D1), it follows:

$$\left[\frac{\partial Z}{\partial \xi}\left(\frac{\partial Z}{\partial t}\right) + \frac{\partial Z}{\partial \tau}\left(\frac{\partial \tau}{\partial t}\right)\right] - Kx_n\frac{\partial Z}{\partial \xi}\left(\frac{\partial \xi}{\partial x_n}\right) - D\left[\frac{\partial^2 Z}{\partial \xi^2}\left(\frac{\partial \xi}{\partial x_n}\right)^2 + \frac{\partial Z}{\partial \xi}\left(\frac{\partial^2 \xi}{\partial x_n^2}\right)\right] = 0 \tag{D9}$$

The term $(\partial^2\xi/\partial x_n^2)$ vanishes because $\partial\xi/\partial x_n$ depends only on time t.

By posing in evidence the term $\partial Z/\partial\xi$ Eq. (D9) becomes

$$\frac{\partial Z}{\partial t}\left(\frac{\partial \tau}{\partial t}\right) + \frac{\partial Z}{\partial \xi}\left[\frac{\partial \xi}{\partial t} - Kx_n\left(\frac{\partial \xi}{\partial x_n}\right)\right] + - D\left(\frac{\partial \xi}{\partial x_n}\right)^2\frac{\partial^2 Z}{\partial \xi^2} = 0 \tag{D10}$$

and by using Eqs. (D6) and (D7)

$$\frac{\partial Z}{\partial \tau}\left(\frac{\partial \tau}{\partial t}\right) + \frac{\partial Z}{\partial \xi}[x_n f'(t) - Kx_n f(t)] + - Df^2(t)\frac{\partial^2 Z}{\partial \xi^2} = 0 \tag{D11}$$

If we choose the function $f(t)$ such that

$$x_n f^Y(t) - K\, x_n f(t) = 0 \tag{D12}$$

it follows: $f^Y(t) = Kf(t)$, and $\int_{t_o}^{t}((\mathrm{d}f)/f)\int_{t_o}^{t} K\,\mathrm{d}t$.

By integrating

$$f(t) = \exp\left[\int_{t_o}^{t} K\,\mathrm{d}t\right] = \mathrm{SR} \tag{D13}$$

and by posing $f(t_o) = 1$ it results

$$\xi(x_n, t) = x_n f(t) = x_n \mathrm{SR} \tag{D14}$$

and Eq. (D11) can be written as

$$\frac{\partial Z}{\partial \tau}\left(\frac{\mathrm{d}\tau}{\mathrm{d}t}\right) - D\mathrm{SR}^2\frac{\partial^2 Z}{\partial \xi^2} = 0 \tag{D15}$$

if we assume that $(\mathrm{d}\tau/\mathrm{d}t) = \mathrm{SR}^2$ Eq. (D15) becomes

$$\frac{\partial Z}{\partial \tau} - D\frac{\partial^2 Z}{\partial \xi^2} = 0 \tag{D16}$$

where

$$\xi(x_n, t) = x_n \mathrm{SR} \tag{D17}$$

integrating $\mathrm{d}\tau/\mathrm{d}t$ in $\mathrm{d}t$, it results

$$\tau = \int_{t_o=0}^{t} \mathrm{SR}^2\,\mathrm{d}t = t\overline{\mathrm{SR}^2} \tag{D18}$$

Eq. (D16) is the classical unsteady diffusion equation that can be solved by making the classical Boltzmann variable transformation

$$\eta = \frac{\xi}{\sqrt{4D\tau}} \tag{D19}$$

that means

$$\left\{\frac{\partial \eta}{\partial \xi} = \frac{1}{\sqrt{4D\tau}}, \frac{\partial \eta}{\partial \tau} = -\frac{\eta}{2\tau}\right\} \tag{D20}$$

By substituting Eq. (D19) in Eq. (D16), it results

$$\frac{\partial Z}{\partial \eta}\left(\frac{\partial \eta}{\partial \tau}\right) - D\left(\frac{\partial \eta}{\partial \xi}\right)^2\frac{\partial^2 Z}{\partial \eta^2} = 0 \tag{D21}$$

and by using Eq. (D20) we obtain

$$\frac{\partial Z}{\partial \eta}\left(-\frac{\eta}{2\tau}\right) - D\left(\frac{1}{\sqrt{4D\tau}}\right)^2\frac{\partial^2 Z}{\partial \eta^2} = 0 \tag{D22}$$

therefore we obtain

$$2\eta\frac{\partial Z}{\partial \eta} + \frac{\partial^2 Z}{\partial \eta^2} = 0 \tag{D23}$$

or in a different form

$$\frac{\mathrm{d}^2 Z}{\mathrm{d}\eta^2} = -2\frac{\mathrm{d}Z}{\mathrm{d}\eta} \tag{D24}$$

Introducing $G = (\mathrm{d}Z/\mathrm{d}\eta)$ Eq. (D24) becomes

$$\frac{\mathrm{d}G}{\mathrm{d}\eta} = -2\eta G \tag{D25}$$

by the separation of the variables it results in

$$\frac{\mathrm{d}G}{G} = -2\eta\,\mathrm{d}\eta \tag{D26}$$

and integrating $G = c\,\mathrm{e}^{-\eta^2}$. Substituting G and integrating between $\eta = 0(Z_o = 0)$ and η

$$\int_{Z_o}^{Z}\mathrm{d}Z = c\int_0^{\eta}\mathrm{e}^{-\eta^2}\,\mathrm{d}\eta \tag{D27}$$

and finally

$$Z - Z_o = c\frac{\sqrt{\pi}}{2}erf(\eta) \tag{D28}$$

where

$$\mathrm{erf}(\eta) = \frac{2}{\sqrt{\pi}}\int_0^{\eta}\mathrm{e}^{-\eta^2}\,\mathrm{d}\eta$$

is the error function.

Taking into account Eqs. (D19) and (D17)

$$Z - Z_o = c\frac{\sqrt{\pi}}{2}\mathrm{erf}\left(\frac{\xi}{\sqrt{4D\tau}}\right) = c\frac{\sqrt{\pi}}{2}\mathrm{erf}\left(\frac{x_n\mathrm{SR}}{\sqrt{4D\tau}}\right) \tag{D29}$$

By evaluating Eq. (D29) at $x_n = \infty(\mathrm{erf}(\infty) = 1)$, it is possible to calculate $Z = Z_\infty$, and to determine the constant $c = (2/\sqrt{\pi})(Z_\infty - Z_o)$.

Eq. (D29) becomes

$$\frac{Z - Z_o}{Z_\infty - Z_o} = \mathrm{erf}\left(\frac{x_n \mathrm{SR}}{\sqrt{4D\tau}}\right) \tag{D30}$$

and by Eq. (D18)

$$\frac{Z - Z_o}{Z_\infty - Z_o} = \mathrm{erf}\left(\frac{x_n}{\sqrt{4D\tau}} \frac{\mathrm{SR}}{\sqrt{\overline{\mathrm{SR}^2}}}\right) \tag{D31}$$

If we introduce the quantity $\delta_{0.9}$, named mixing layer thickness, as the distance from the origin such that

$$Z - Z_o = 0.9(Z_\infty - Z_o)$$

Eq. (D31) can be written as

$$\frac{Z - Z_o}{Z_\infty - Z_o} = \mathrm{erf}\left(\frac{\delta_{0.9}}{\sqrt{4D\tau}} \frac{\mathrm{SR}}{\sqrt{\overline{\mathrm{SR}^2}}}\right) \tag{D32}$$

The value of $\delta_{0.9}$ can be calculated by considering that $\mathrm{erf}(1) \cong 0.9$. This is

$$1 = \frac{\delta_{0.9}}{\sqrt{4Dt}} \frac{\mathrm{SR}}{\sqrt{\overline{\mathrm{SR}^2}}}$$

and, as a consequence

$$\boxed{\delta_{0.9} = \sqrt{4Dt} \frac{\sqrt{\overline{\mathrm{SR}^2}}}{\mathrm{SR}}} \tag{D33}$$

By using the mixing layer thickness value of Eq. (D33) it is possible to write Eq. (32) in a more compact form

$$\frac{Z - Z_o}{Z_\infty - Z_o} = \mathrm{erf}\left(\frac{x_n}{\delta_{0.9}}\right) \tag{D34}$$

Appendix E

Due to the linearity of the conservation equation for the mixing fraction, Z, a superposition principle can be applied. This is very useful if the initial conditions for Z are such as those depicted in the right side of the figure above. In this case the mixing fraction can be decomposed into two contributions

$$Z = Z_1 - Z_2 \tag{E1}$$

The initial conditions for these components are shown in the left and central plots.

The mixing fraction Z is, then, given by the equation reported in the lower right side of Fig. 22 . It is the difference of two error functions of the two adimensional variables $\xi_1 = x/\delta_1$ and $\xi_2 = ((x - \Delta_n))/\delta_2$.

If $\Delta_n \to \infty$ then $\mathrm{erf}(\xi_2) = -1$ and the mixing fraction is the same of the isolated diffusive layer $Z = (1/2)(1 + \mathrm{erf}(\xi))$. In this case the diffusive flow $J_{\Delta_n \to \infty}$ over an unitary (at $t = 0$) surface at $x = 0$ can be obtained by the equation

$$J_{\Delta_n \to \infty} = -\rho D \frac{\partial Z}{\partial x} \mathrm{SR} \tag{E2}$$

In fact, in the not stirred case, the diffusive flow is given, due to the Fick law, by $-\rho D(\partial Z/\partial x)$. If the stirring has to be taken into account this quantity has to be multiplied by the stirring ratio SR that represents the extent at the time t of a surface unitary at $t = 0$.

Since

$$\frac{\mathrm{d}}{\mathrm{d}\xi}\mathrm{erf}(\xi) = \frac{2}{\sqrt{\pi}} \mathrm{e}^{-\xi} \tag{E3}$$

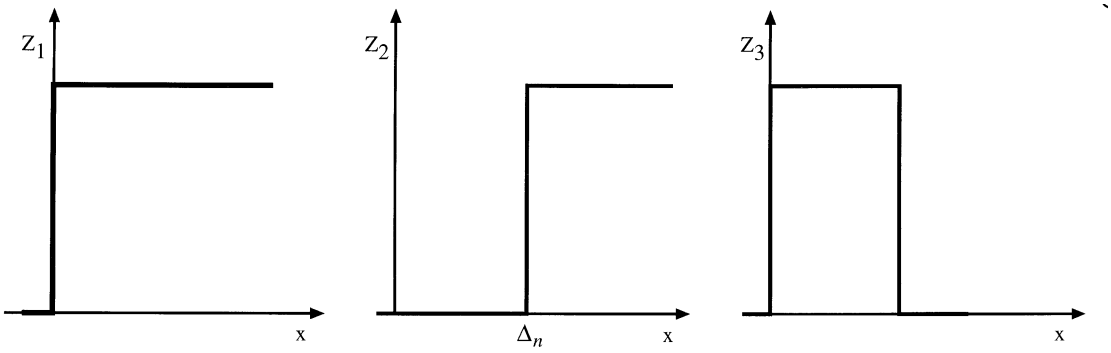

$$Z_1 = \frac{1}{2}\left[1 + erf(\xi_1)\right] \qquad \xi_1 = x/\delta_1 \qquad J_1\big|_{x=0} = -\rho\mathcal{D}\frac{1}{\pi}\frac{SR_1}{\delta_1}$$

$$Z_2 = \frac{1}{2}\left[\left(1 + erf(\xi_2)\right)\right] \qquad \xi_2 = \left(x - \Delta_n\right)/\delta_n \qquad J_2\big|_{x=0} = -\rho\mathcal{D}\frac{1}{\pi}\frac{SR_2}{\delta_2}\exp\left(-\frac{\Delta_n}{\delta_2}\right)$$

$$Z = \frac{1}{2}\left(erf\left(\xi_1\right) - erf\left(\xi_2\right)\right) \qquad J_{\Delta_n}\big|_{x=0} \cong \frac{\rho\mathcal{D}}{\sqrt{\pi}}\frac{SR}{\delta_m}\left[1 - \exp\left(-\frac{\Delta_n}{\delta_m}\right)\right]$$

Fig. 22. Decomposition of mixing fraction Z_3 in Z_1 and Z_2 contributions.

$$\frac{\mathrm{d}\xi}{\mathrm{d}x} = \frac{\mathrm{d}}{\mathrm{d}x}\left(\frac{x}{\delta}\right) = \frac{1}{\delta}$$

it follows that

$$\left.\frac{\partial Z}{\partial \mathrm{x}}\right|_{\xi=0} = \frac{\partial Z}{\partial \xi}\frac{\partial \xi}{\partial x} = \frac{1}{2}\left(\frac{2}{\sqrt{\pi}}\right)\mathrm{e}^{-\xi}\Big|_{\xi=0}\frac{1}{\delta} = \frac{1}{\sqrt{\pi}}\frac{1}{\delta} \qquad \text{(E4)}$$

and the diffusive flow, in the case of an isolated layer becomes

$$J_{\Delta_n\to\infty} = -\rho D\frac{1}{\sqrt{\pi}}\frac{\mathrm{SR}}{\delta_m} \qquad \text{(E5)}$$

This expression shows the twofold influence of the stirring (i.e. of the fluid-dynamics) on the mass exchange between two gaseous layers. In fact, if the stirring is present the diffusive flow increases because the material surface increases (and this taken in account by the SR term in Eq. (E5)). Furthermore, the mixing layer thickness (expressed by the δ_m term) is lowered according to the expression

$$\delta_{\mathrm{stirred}} = \delta_{\mathrm{isolated}}\frac{\sqrt{\overline{\mathrm{SR}^2}}}{\mathrm{SR}} = \delta_{\mathrm{isolated}}\gamma \qquad \text{(E6)}$$

where the γ factor is generally lower than 1. Both these effects increase the diffusive flow in the stirred case with respect to the isolated one.

The diffusive flow in the case of a double diffusive layer ($J_{\Delta n}$) can be obtained by substituting ($\partial Z/\partial x$) in Eq. (E2) with the one relative to the double layer

$$\begin{aligned}\frac{\partial z}{\partial x} &= \frac{1}{2}\left(\frac{\partial \mathrm{erf}(\xi_1)}{\partial \xi_1}\frac{\partial \xi_1}{\partial x} - \frac{\partial \mathrm{erf}(\xi_2)}{\partial \xi_2}\frac{\partial \xi_2}{\partial x}\right)\\ &= \frac{1}{2}\left(\frac{2}{\sqrt{\pi}}\,\mathrm{e}^{-\xi_1}\frac{1}{\delta_1} - \frac{2}{\sqrt{\pi}}\,\mathrm{e}^{-\xi_2}\frac{1}{\delta_2}\right)\\ &= \frac{1}{\sqrt{\pi}}\frac{1}{\delta}\left[1-\exp\left(-\frac{\Delta_n}{\delta}\right)\right]\end{aligned}$$

by assuming $\delta_1 = \delta_2$, that is the two diffusive layers would evolve in the isolated case nearly equally

$$J_{\Delta_n} = -\rho D\mathrm{SR}\frac{\partial Z}{\partial x} = -\frac{\rho D}{\sqrt{\pi}}\frac{\mathrm{SR}}{\delta_n}\left[1-\exp\left(-\frac{\Delta_n}{\delta}\right)\right] \qquad \text{(E7)}$$

It is possible to define the quantity C_{sat}

$$C_{\mathrm{sat}} = \frac{J_{\Delta_n}}{J_{\Delta_n\to\infty}} = 1-\exp\left(-\frac{\Delta_n}{\delta}\right) \qquad \text{(E8)}$$

It is

$$0 \le C_{\mathrm{sat}} \le 1$$

In the case $\Delta_n \to \infty$ (isolated mixing layers) C_{sat} value is 1. Lower values are relative to progressively more interacting mixing layers.

References

[1] Burke SP, Schumann TEW. Ind Engng Chem 1928;20:998. Reprinted in Proc Combust Inst 1965;1: 2–11.
[2] Tsuji H. Prog Energy Combust Sci 1982;8:93–119.
[3] Tsuji H, Yamaoka I. Proc Combust Inst 1967;11:979–84.
[4] Peters N. Length scales in laminar and turbulent flames numerical approaches to combustion modeling. Oran ES, Boris JP, editors, 1989.
[5] Liñan A. Acta astronautica, vol. 1. New York: Pergamon Press; 1974. p. 1007–39.
[6] Peters N. Combust Sci Technol 1983;30:1–17.
[7] Bilger RW. Combust Sci Technol 1976;13:155–70.
[8] Edelman RB, Fortune OF, Weilerstein G, Cochran TH, Haggard Jr JB. Proc Combust Inst 1973;14:399–412.
[9] Aref H. J Fluid Mech 1984;143:1–21.
[10] Chella J, Ottino JM. Chem Engng Sci 1984;39:551–67.
[11] Kerstein AR, Law CK. Proc Combust Inst 1982;19:961–9.
[12] Ottino JM. The kinematics of mixing stretching, chaos and transport. Cambridge: Cambridge University Press; 1989.
[13] Williams FA. Combustion theory. Menlo Park, CA: Benjamin/Cummings; 1985.
[14] Kuo K. Principles of combustion. New York: Wiley; 1986.
[15] Chigier N. Energy, combustion and environment. New York: McGraw-Hill; 1981.
[16] Barnard JA, Bradley JN. Flame and combustion. London: Chapman and Hall; 1985.
[17] Ottino JM. J Fluid Mech 1982;114:83–103.
[18] Crowe CT, Chung JN, Troutt TR. Prog Energy Combust Sci 1988;14:171–94.
[19] Rosner DE. Transport processes in chemically reacting flow systems. Boston, MA: Butterworths; 1986. p. 123.
[20] Chaiken J, Chu CK, Tabor M, Tan QM. Phys Fluids 1987;30:687–94.
[21] Cavaliere A, El-Naggar M, Ragucci R. Int J Heat Mass Transfer 1995;38:317–29.
[22] Pope SB, Int. J Engng Sci 1988;5:445–69.
[23] Gibson CH. Phys Fluids 1968;11:2305–15.
[24] Cavaliere A, De Felice G, Denaro F, Meola C. Proceedings of The First European Congress on Chemical Engineering. European Federation Chemical Engineering, vol. 3, 1997. p. 1719–27
[25] Marble FE, Broadwell JE. Project Squid TRW-9-PU, Project Squid Headquarters, Chaffee Hall, Purdue University, 1977.
[26] Candel S, Martin JP. Coherent flame modelling of chemical reactions in a turbulent mixing layer. In: Warnatz J, Jger W, editors. Complex chemical reaction systems, Berlin: Springer; 1987. p. 386–98.
[27] Darabiha N, Giovangigli V, Trouvé A, Candel S, Esposito E. Coherent flame description of turbulent premixed ducted flames. In: Borghi R, Murthy SNB, editors. Turbulent reactive flows, New York: Springer; 1989. p. 591–637.
[28] Maistret E, Darabiha N, Poinsot T, Veynante D, Lacas F, Candel S, Esposito E. Recent developments in the coherent flamelet description of turbulent combustion. In: Dervieux A, Larrouturou B, editors. Numerical combustion, Berlin: Springer; 1989. p. 98–117.
[29] Veynante D, Lacas F, Maistret E, Candel S. Coherent flame model in non-uniformly premixed turbulent flames, Turbulent shear flows, vol. 7. Berlin: Springer; 1991. p. 367–78.

[30] Fichot F, Delhaye B, Veynante D, Candel S. Proc Combust Inst 1994;25:1273–81.
[31] Trouvé A, Poinsot T. J Fluid Mech 1994;278:1–31.
[32] Vervish L, Bidaux , Bray KNC, Kollmann W. Phys Fluids 1995;A7(10):2496–503.
[33] Candel SM, Veynante D, Lacas FF, Maistret E, Darabiha N, Poinsot T. Coherent flame model, application and recent extension. In: Larrouturou B, editor. Recent advances in combustion modelling, Series on Advances in Mathematics for Applied Sciences. Singapore: World Scientific; 1990.
[34] Muller CM, Breitbach H, Peters N. Proc Combust Inst 1994;25:1099–106.
[35] Kerstein AR, Ashurst WT, Williams FA. Phys Rev A 1988;37:2728–31.
[36] Peters N. J Fluid Mech 1992;242:611–29.
[37] Vervish L, Poinsot T. Annu Rev Fluid Mech 1998;30:655–91.
[38] Van Kalmthout E, Veynante D, Candel S. Proc Combust Inst 1996;26:35–42.
[39] Meyers RE, O'Brien EE. Combust Sci Technol 1981;26:123–34.
[40] Bilger RW. Prog Energy Combust Sci 1976;1:87–109.
[41] Peters N. Prog Energy Combust Sci 1984;10:319–39.
[42] Stepowski D. Prog Energy Combust Sci 1992;18:463–91.
[43] Masri AR, Dibble RW, Barlow J. Prog Energy Combust Sci 1996;22:307–62.
[44] Drake MC, Lapp M, Penney CM, Warshaw S, Gerhold BW. Proc Combust Inst 1981;18:1521–31.
[45] Frank JH, Lyons KM, Marran DF, Long MB, Starner SH, Bilger RW. Proc Combust Inst 1994;25:1159–66.
[46] Kelman JB, Masri AR, Starner SH, Bilger RW. Proc Combust Inst 1994;25:1141–7.
[47] Everest DA, Feikema DA, Driscoll JF. Proc Combust Inst 1996;26:129–36.
[48] Tait NP, Greenhalgh DA. Proc Combust Inst 1992;26:1621–8.
[49] Hanson RK. Proc Combust Inst 1986;18:1677–91.
[50] Bush WB, Fendell FE. J Fluid Mech 1974;64:701–24.
[51] Bilger RW. Combust Sci Technol 1976;13:155.
[52] Kent JH, Bilger RW. Proc Combust Inst 1976;14:615–25.
[53] Eickhoff H, Grethe K. Combust Flame 1979;35:267–75.
[54] Fendel CR, Keck JC. J Fluid Mech 1972;56:81–95.
[55] Frank-Kamenetski DA. Diffusion and heat transfer in chemical kinetics. New York: Plenum Press; 1973.
[56] Williams FA. Annu Rev Fluid Mech 1973;11:1328.
[57] Buckmaster JD, Ludford GSS. Theory of laminar flames. Cambridge: Cambridge University Press; 1982.
[58] Seshadri K, Peters N. Combust Flame 1988;73:23–44.
[59] Peters N. Proc Combust Inst 1986;21:1231–50.
[60] Liew SK, Bray KNC, Moss JB. Combust Sci Technol 1981;27:69–73.
[61] Smooke MD, Xu Y, Zurn RM, Lin P, Frank JH, Long MB. Proc Combust Inst 1992;24:813–21.
[62] Warnatz J. Proc Combust Inst 1984;20:845–56.
[63] Behrendt F, Rogg B, Warnatz J. Proc Combust Inst 1986;18:1533–42.
[64] Givi P. Progr Energy Combust Sci 1989;15:1–107.
[65] Tennekes H, Lumley JL. A first course in turbulence. Boston, MA: MIT Press; 1972.
[66] Takeno T. Proc Combust Inst 1994;25:1061–73.
[67] Sirignano WA. Progr Energy Combust Sci 1983;9:291.
[68] Sung CH, Zhu DL, Law CK. Proc Combust Inst 1988;27:2559–66.
[69] Mills K, Matalon M. Proc Combust Inst 1998;27:2535–42.
[70] Ronney P. Proc Combust Inst 1988;27:2485–506.
[71] Yamamoto K, Hirano T, Ishizuka S. Proc Combust Inst 1996;26:1129–35.
[72] Boothman D, Lawton J, Melinek SJ, Weinberg F. Proc Combust Inst 1969;12:969–78.
[73] Coats CM, Zhao H. Proc Combust Inst 1988;22:685–92.
[74] Chen LD, Seaba JP, Roquemore WM, Goss LP. Proc Combust Inst 1988;22:677–84.
[75] Lingens A, Neemann K, Meyer J, Schreiber M. Proc Combust Inst 1996;26:1053–61.
[76] Davis RW, Moore EF, Roquemore WM, Chen LD, Vilimpoc V, Goss LP. Combust Flame 1991;83:263–70.
[77] Cussler EL. Multicomponent diffusion. Chemical Engineering Monographs, vol. 3. Amsterdam: Elsevier; 1976.
[78] Spalding DB. ARS J 1961;31:76.
[79] Jain VK, Mukunda HS. Combust Sci Technol 1969;1:105–17.
[80] Dixon-Lewis G, David T, Gaskell PH, Fukutani S, Jinno H, Miller JA, Kee RJ, Smooke MD, Peters N, Effelsberg E, Warnatz J, Beherendt F. Proc Combust Inst 1984;20:1893–904.
[81] Sick V, Arnold A, Diesel E, Dreier T, Ketterle W, Lange B, Wolfrum J, Thiele KU, Behrendt F, Warnatz J. Proc Combust Inst 1990;23:495–501.
[82] Dreier T, Langer B, Wolfrum J, Zahn M, Beherendt F, Warnatz J. Proc Combust Inst 1986;21:1729–36.
[83] Yamaoka I, Tsuji H. Proc Combust Inst 1974;15:637–44.
[84] Law CK. Proc Combust Inst 1988;22:1381–402.
[85] Dixon-Lewis G. Proc Combust Inst 1990;23:305–24.
[86] Papas P, Glassman I, Law CK. Proc Combust Inst 1994;25:1333–9.
[87] Chelliah HK, Law CK, Ueda T, Smooke MD, Williams FA. Proc Combust Inst 1990;23:503–11.
[88] Evans S, Simmons RF. Proc Combust Inst 1988;22:1433–9.
[89] Barlow RS, Dibble RW, Starner SH, Bilger RW. Proc Combust Inst 1990;23:583–9.
[90] Barlow RS, Dibble RW, Chen JH, Lucht RP. Combust Flame 1990;72:255–69.
[91] Dixon-Lewis G, Missaghi M. Proc Combust Inst 1988;22:1461–70.
[92] Gutheil E, Williams FA. Proc Combust Inst 1990;23:513–21.
[93] Ishizuka S, Tsuji H. Proc Combust Inst 1979;18:695–703.
[94] Sjogren A. Proc Combust Inst 1973;14:919–27.
[95] Smooke MD, Seshadri K, Puri IK. Proc Combust Inst 1988;22:1555–63.
[96] Tanoff MA, Smooke MD, Osborne RJ, Brown TM, Pitz RW. Proc Combust Inst 1996;26:1121–8.
[97] Bruel P, Rogg B, Bray KN. Proc Combust Inst 1973;23:759–66.
[98] Yiguag J. The First Asia–Pacific Conference on Combustion, Osaka, Japan Proceedings, 1997. p. 460.
[99] Sung CJ, Law CK. Proc Combust Inst 1998;27:1411–8.
[100] Breitbatch H, Goettgens J, Mauss F, Pitsch H, Peters N. Proc Combust Inst 1994;25:1357–64.
[101] Wang H, Du DX, Sung CJ, Law CK. Proc Combust Inst 1996;26:2359–68.
[102] Cheatham S, Matalon M. Proc Combust Inst 1996;26:1063–70.

[103] Kerstein AR. Proc Combust Inst 1984;20:1915–23.
[104] Strahle WC. Proc Combust Inst 1965;10:253–7.
[105] Im HG, Law CK, Kim JS, Williams FA. Combust Flame 1995;100:21–30.
[106] Kim JS, Williams FA. Combust Flame 1994;98:279–99.
[107] Ghoniem AF, Soteriou MC, Knio OM, Cetegen B. Proc Combust Inst 1992;24:223–30.
[108] Mauss F, Keller D, Peters N. Proc Combust Inst 1990;23:693–8.
[109] Barlow RS, Chen JY. Proc Combust Inst 1992;24:231–7.
[110] Brown TM, Pitz RW, Sung CJ. Proc Combust Inst 1998;27:703–10.
[111] Saitoh T, Otsuka Y. Combust Sci Technol 1976;12:135–46.
[112] Kistler JS, Sung CJ, Kreutz TG, Law CW, Nishioka M. Proc Combust Inst 1996;26:113–20.
[113] Beige D, Leonard A, Wiggins S. Phys Fluid A 1991;35:1039–50.
[114] Carrier GF, Fendell FE, Marble FE. SIAM J Appl Math 1975;28:463–500.
[115] Tryggavson G, Dahm WJA. Combust Flame 1991;83:207–20.
[116] Echekki T, Chen JM, Gran I. Proc Combust Inst 1996;26:855–63.
[117] Cetegen BM, Bogue DR. Combust Flame 1991;86:359–70.
[118] Spalding DB. Combustion and mass transfer. New York: Pergamon Press; 1979.
[119] Schlichting M. Boundary layer theory. New York: McGraw–Hill; 1968.
[120] Shu Z, Krass BJ, Choi CW, Aggarwal SK, Katta VR, Puri IK. Proc Combust Inst 1998;27:625–32.
[121] McEnally CS, Schaffer AM, Long MB, Pfefferle LD, Smooke MD, Colket MB, Hall RJ. Proc Combust Inst 1998;27:1497–506.
[122] De Juliis S, Cignoli F, Benecchi S, Zizak G. Proc Combust Inst 1998;27:1549–56.
[123] Ho CM, Huerre P. Annu Rev Fluid Mech 1984;16:365–424.
[124] Raghunandan BN, Yogesh GP. Proc Combust Inst 1988;22:1501–7.
[125] Warpinski NR, Nagib HM. AIAA J 1972;10(4):1204–10.
[126] Cavaliere A, Ragucci R, Vanacore G, Venitozzi C. Proceedings of The Fifth Conference International of Fluid Mechanics, Cairo, 1995. p. 151–62.
[127] Samuelsen GS, Starkman ES. Combust Sci Technol 1972;5:31–41.
[128] Beér JM, Chigier NA. Combustion aerodynamics. London: Applied Science; 1972.
[129] Lilley DG. Swirling flows. London: Applied Science, 1977.
[130] Durst F, Melling A, Whitelaw JH. J Fluid Mech 1974;64:111–28.
[131] Edelman RB, Harsha PT. Progr Energy Combust Sci 1978;4:1–62.
[132] Wu K, Essenhigh R. Proc Combust Inst 1984;20:1925–32.
[133] Makel DB, Kennedy IM. Combust Sci Technol 1994;97:303–30.
[134] Dold JW. Prog Astron Aeronaut 1988;131:240–8.
[135] Dold JW. Triple flames and flaming vortices; invited review. ERCOFTAC Bull 1994;20:38–42.
[136] Buckmaster J, Matalon M. Proc Combust Inst 1988;22:1527–35.
[137] Dold JW. Combust Flame 1989;76:71–88.
[138] Domingo P, Vervish L. Proc Combust Inst 1996;26:223–40.
[139] Muller CM, Breitbach H, Peters N. Proc Combust Inst 1992;25:1099–106.
[140] Kioni PN, Rogg B, Bray KNC, Liñan A. Combust Flame 1993;95:276–90.
[141] Lee BJ, Chung SH. Combust Flame 1997;109:163–72.
[142] Plessing T, Terhoeven P, Peters N, Mansour MS. Combust Flame 1998;115:335–53.
[143] Buckmaster JD, Weber R. Proc Combust Inst 1996;26:1143–9.
[144] Wichman IS, Lakkaraju N, Ramadan B. Combust Sci Technol 1997;127:141–65.
[145] Daou J, Liñan A. Proc Combust Inst 1998;27:667–74.
[146] Renard PH, Thévenin D, Rolon C, Candel S. Prog Energy Combust Sci 2000;26:225–82.
[147] Marble FE. Growth of a diffusion flame in the field of a vortex. In: Casci C, Bruno C, editors. Recent advances in aerospace sciences. New York: Plenum Press; 1985. p. 395–413.
[148] Laverdant AM, Candel S. Combust Sci Technol 1988;60:79.
[149] Delhaye D, Veynante D, Candel S, Ha Minh H. Theor Comput Fluid Dyn 1994;6:67–87.
[150] Ashurst WT, Williams FA. Proc Combust Inst 1991;23:543–50.
[151] Katta VR, Carter CD, Fiechtner GJ, Roquemore WM, Gord JR, Rolon JC. Proc Combust Inst 1998;27:587–94.
[152] Ashurst WT, Dervieux A, Larrouturou B. Lectures notes in physics, vol. 351. Berlin: Springer; 1989.
[153] Soteriou M. Proc Combust Inst 1998;27:1213–20.
[154] Katta VR, Roquemore WM. Combust Flame 1995;100:61–70.
[155] Karagozian AR, Marble FE. Combust Sci Technol 1986;45:65–84.
[156] Chen SJ, Dahm WJA. Proc Combust Inst 1998;27:2579–86.
[157] Takahashi F, Katta V. Proc Combust Inst 1996;26:1151–60.
[158] Thevenin D, Rolon JC, Renard PH, Kendrick DW, Veynante D, Candel S. Proc Combust Inst 1996;26:1079–86.
[159] Rolon JC, Aguerre F, Candel S. Combust Flame 1995;100:422–9.
[160] Patnaik G, Kailasanath K. Proc Combust Inst 1998;27:711–8.
[161] Thévenin D, Renard PH, Rolon JC, Candel S. Proc Combust Inst 1998;27:719–26.
[162] Mathew J. Proc Combust Inst 1998;27:1207–12.
[163] Mueller CJ, Schefer RW. Proc Combust Inst 1998;27:1105–12.
[164] Rangel R, Sirignano WA. 27th Aerospace Meeting, AIAA 89-0128 1988. p. 1–19.
[165] Husain AKMF. J Fluid Mech 1986;173:303–56.
[166] Tennekes H, Lumley JL. A first course in turbulence. Boston, MA: MIT Press; 1972.
[167] Kerr OS, Dold JW. J Fluid Mech 1994;276:306–16.
[168] Dold JW, Kerr OS, Nikolova IP. Combust Flame 1995;100:359–65.
[169] Dold JW. Triple flame as agent for restructuring of diffusion flame. Proceedings of Zel'dovich Memorial, Institute of Structural Macro-kinetics, Chernogolovca, vol. 7, 1994.
[170] Gibson CH. Kolmogorov similarity hypotheses for scalar fields, sampling intermittent turbulent mixing in ocean and galaxy. In: Hunt JCR, Phillips OM, Williams D, editors. Turbulence and stochastic processes, Kolmogorov's ideas 50 years on. University Press: Royal Society; 1991. p. 149–64.

[171] Gibson CH. J Fluid Mech 1986;168:89–117.
[172] Lee JHS, Moen IO. Prog Energy Combust Sci 1980;6:359–89.
[173] Cavaliere A, El-Naggar M, Ragucci R. Combust Flame 1994;99:679–86.
[174] Cavaliere A, de Felice G, Denaro F, Meola C. Proceedings of computational methods and experimental measurements. Berlin: Springer; 1993. p. 135–50.
[175] Husain MS, Bridges JE, Hussain F. Transport phenomena in turbulent flows. New York: Hemisphere; 1988. p. 111.
[176] Takeno T. Proc Combust Inst 1994;25:1061–73.
[177] Takahashi F, Mizamoto M, Ikai S. Combust Flame 1982;48:85–95.
[178] Coats CM, Zhao M. Proc Combust Inst 1988;22:685–92.
[179] Ellzey JL, Oran ES. Proc Combust Inst 1990;23:1635–40.
[180] Yamashita H, Shimada M, Takeno T. Proc Combust Inst 1996;26:27–34.
[181] Lee BJ, Kim JS, Chung SH. Proc Combust Inst 1994;25:1175–81.
[182] Clemens NT, Paul PM. Combust Flame 1995;102:271–84.
[183] Cha MS, Chung SH. Proc Combust Inst 1996;26:121–8.
[184] Everest DA, Driscoll JF, Dahm WJA, Feikema DA. Combust Flame 1995;101:58–68.
[185] Everest DA, Feikema DA, Driscoll JF. Proc Combust Inst 1996;26:129–36.
[186] Vuillermoz P, Oran ES, Kailasanath K. Proc Combust Inst 1992;24:395–403.
[187] Grinstein F, Kailasanath K. Proc Combust Inst 1996;26:91–96.
[188] Kolman W, Chen JH. Proc Combust Inst 1992;25:1091–8.
[189] Mahalingam S, Chen JH, Vervish L. Combust Flame 1995;102:285–97.
[190] Candel SM, Poinsot T. Combust Sci Technol 1990;70:1–15.
[191] Aris R. Vectors, tensors and basic equations of fluid-mechanics. Englewood Cliffs, NJ: Prentice Hall; 1962.